POST-GRADUATE PROGRAM IN PHYSICS
UNIVERSIDADE FEDERAL DO RIO GRANDE DO SUL

Classic models for the study of microscopic friction
Modelos clássicos para o estudo do atrito microscópico [1]

Student: Maria Luján Iglesias

Thesis submitted to the Universidade Federal do Rio Grande do Sul as a partial requirement to obtain the degree of Doctor in Sciences, under the supervision of Prof. Dr. Sebastian Gonçalves (Institute of Physics - UFRGS - Porto Alegre (RS), Brasil).

October, 2018

[1] Project financed by the Scholarship Program Latin American Physics Center and National Center for Scientific and Technological Development CLAF/CNPq.

I can believe things that are true
and things that aren't true and
I can believe things where nobody
knows if they're true or not
Neil Gaiman- American Gods

Acknowledgment

I would like to thank my supervisor Prof. Sebastián Gonçalves for his guidance, encouragement and support in overcoming numerous obstacles I have faced through my research.

To Prof. V.M. Kenkre and N. Tiwari for the collaboration and contribution to this work.

I am also grateful to the CLAF (Centro Latinoamericano de Física) and CNPq (Conselho Nacional de Desenvolvimento Científico e Tecnológico) for the scholarship.

To my friends and dear family for the continuous encouragement and to my fiance, Rafael, for his patience and unconditional support.

Resumo

O atrito é um fenômeno extremamente onipresente, a ponto de que a maior parte do tempo não percebemos como isso afeta nossas vidas, desde pequenos detalhes até aspectos fundamentais. Geralmente é considerado um problema relacionado com a perda de energia e desgaste das peças das máquinas, mas sem sua existência não ouviríamos o violino, as unhas seriam inúteis, e a vida não poderia ser possível, pois num regime sem desgaste, o equilíbrio térmico seria inalcançável. As técnicas experimentais atuais capazes de estudar a força de atrito, abriram um novo campo de pesquisa envolvendo escalas de comprimento atômico, chamado de nano-tribologia. Apesar disso, a origem microscópica da força de atrito permanece principalmente não resolvida até hoje. Nesta tese de doutorado, foi estudada a base da origem da força de atrito, primeiro investigando sua dependência com a velocidade através do conhecido modelo de Prandtl-Tomlinson para temperatura igual a zero. A essência da troca de energia, que poderia explicar o surgimento do atrito foi investigada pela dinâmica entre duas partículas. Uma ligada a uma mola e a outra lançada em sua direção com certa velocidade, sendo a interação entre elas do tipo gaussiano (curto alcance). Para simular um substrato mais realista, o sistema de partículas-mola foi estendido para uma disposição periódica de partículas, independentes entre elas, e a partícula que no primeiro modelo era lançada, foi substituída por uma ponta, geralmente usada para escanear as superfícies no microscópio de força atômica. A principal técnica utilizada foi dinâmica molecular, ferramenta ideal para abordar o estudo da dinâmica de sistemas clássicos de muitas partículas.

Abstract

Friction is an extremely ubiquitous phenomenon, to the point that most of the time we do not realize how it affects our lives, from tiny details to fundamental aspects. It is usually regarded as a nuisance related with the loss of energy and wear of machine parts, but without it, we would not hear the violin, the nails would be useless, and life could not be possible because in a wearless regime, the thermal equilibrium would be unattainable. The current experimental techniques able to study friction forces, opened a new field of research involving atomic length scales, called nano-tribology. Despite this, the microscopic origin of friction force remains mostly unsolved until date. In this PhD thesis, was studied the basis of the origin of the friction force, first investigating its dependence with the velocity through the well-known Prandtl-Tomlinson model for zero temperature. The essence of the energy exchange that could explain the emergence of friction was investigated by the dynamics between two particles. One attached to a spring and the other sliding in its direction with a certain speed. The interaction between them represented by Gaussian potential (short range). To simulate a more realistic substrate, the spring-particle system was extended to a periodic arrangement of particles, independent between them, and the particle that was thrown against it was replaced by a tip, generally used to scan the surfaces on the atomic force microscope. The main used technique was molecular dynamics, an ideal tool to address the study the dynamics of many particles classical systems.

Contents

List of Figures

Structure of the thesis

This thesis is organized as follows: The first chapter is an introduction to the subjects of friction, the origin of its concept, why is important, the macroscopic and microscopic friction, and the first experiments. In the second part of this chapter I describe the modern experimental techniques used to the study of friction. The second chapter presents the theoretical previous research, such as the Prandtl-Tomlinson model and its velocity-friction relation, mostly used to develop the present work, as well as a brief presentation of the Frenkel-Kontorova Model. The third chapter is dedicated to present the specific models proposed in this thesis, and the main technique and algorithms used to solve the differential equations. Chapter four is devoted to the results, and is comprised by three sections: The first one presents our analysis of the dependence of friction with velocity for the Prandtl-Tomlinson Model. The second one, the results of the first model, and the third one, the results of the second model. The last chapter summarizes the results and conclusions of the thesis.

Chapter 1

Introduction

The study of sliding friction is one of the oldest problems in physics, and certainly a very important one from a practical point of view, whose fundamental origin has been studied for centuries and still remains controversial [1, 2, 3]. It was in March 9, 1966, that the word and concept of tribology were first enunciated to an unsuspecting world in the Jost report by the British Department (Ministry) of Education and Science [4]. In it, tribology, derived from the Greek tribos rubbing, was defined as *"The science and technology of interacting surfaces in relative motion - and of associated subjects and practices"*. Largely because of its multidisciplinary nature, the concept of tribology had been universally neglected, or even overlooked. As a direct result of this neglect, the development of mechanical engineering design had been retarded, and vast sums of money had been lost through unnecessary wear and friction and their consequences.

Richard P. Feynmann wrote in 1963 *"It is quite difficult to do accurate quantitative experiments in friction, and the laws of friction are still not analyzed very well, in spite of the enormous engineering value of an accurate analysis"*. Most recently estimates, improved attention to friction and wear would save developed countries up to $1.6\,\%$ of their gross national product, or over $\$100$ billion annually in the US alone [2, 5]. On the other hand, there are situations where it is desired to increase the friction (braking) rather than decrease it. For this reason, having control on friction can come only through a deep understanding of the microscopic bases of it [6] [1, 7, 8, 9]. Low friction surfaces have increased demand for high-technology components such as computer storage systems, small engines and aerospace devices. Without friction there would not be violin music and it would be impossible to walk or drive a car. Nevertheless, many aspects of sliding

friction are still not well understood with what is beginning to emerge an understanding of friction at an atomic level.

But why is so little known on the topic? The answer lies primarily in the fact that friction and wear are surface and interfacial phenomena which occur at a myriad of buried contacts which not only are extremely difficult to characterize, but are continuously evolving as the microscopic irregularities of the sliding surfaces touch and push into one another [10].

Despite that, in the last decades much progress has been made in the fundamental understanding of the origin of friction [11, 12].

Dry friction is perhaps the simplest but most fundamental type of friction in tribology. Involves many interesting and complex physical phenomena,such as adhesion,wetting,atom exchange,elastic and plastic deformation,and various energy damping progresses. The understanding of all these phenomena aims to increase the control over the mechanisms of friction and thus reduce the loss of energy.

In the last years, theoretical models for atomic friction, mostly based on the early work of Prandtl-Tomlinson [13, 14], and Frenkel-Kontorova [15, 16, 17] were proposed. The advantage of such models resides in being simple and yet retaining enough complexity to exhibit interesting features [12, 18, 19, 20, 21, 22, 23, 24]. Such models have allowed to explain essential features of atomic-scale friction, where the dissipated energy and friction force have been revealed indirectly from stick-slip motion.

1.1 Objective

The objective of this doctoral thesis, foremost is to achieve a better understanding of the nanoscopic origin of the frictional force. To achieve this, first, it was studied in depth, the 1D Prandtl-Tomlinson model for $T = 0$ and the dependence of the friction force with velocity. Then, two models were developed. The first consisting in two particles (one free to move and the other attached to a spring) and the second in an arrangement of particles simulating a tip-substrate system in an AFM microscope. These two models try to explain the essence of the energy exchange that could originate the emergence of friction.

1.2 Friction: A very old problem

More than $400.000\,\mathrm{years}$ ago, our hominid ancestors in Algeria, China and Java were making use of friction when they chipped stone tools [26]. By $200.000\,\mathrm{B.C.E.}$, Neanderthals had achieved a clear mastery of friction, generating fire by the rubbing of wood on wood and by the striking of flint stones. Significant developments also occurred $5.000\,\mathrm{years}$ ago : Egyptian tomb drawings suggest that wetting the sand with water may influence the friction between a sled and the sand (Fig. 1.1), although the significance of the person wetting the sand has been much disputed, it was show experimentally [27] that the sliding friction on sand is greatly reduced by the addition of some —but not too much— water. The formation of capillary water bridges increases the shear modulus of the sand, which facilitates the sliding. Too much water, on the other hand, makes the capillary Bridges coalesce, resulting in a decrease of the modulus; and that the friction coefficient increases again. This show that the friction coefficient is directly related to the shear modulus; having important repercussions for the transport of granular materials [28]. This is an important issue, since the transport and handling of granular materials is responsible for around $10\,\%$ of the world energy consumption [29].

Modern tribology began perhaps 500 years ago, when Leonardo da Vinci deduced the laws governing the motion of a rectangular block sliding over a flat surface (Fig. 1.2. (Da Vinci's work had no historical influence, however, because his notebooks remained unpublished for hundreds of years.)

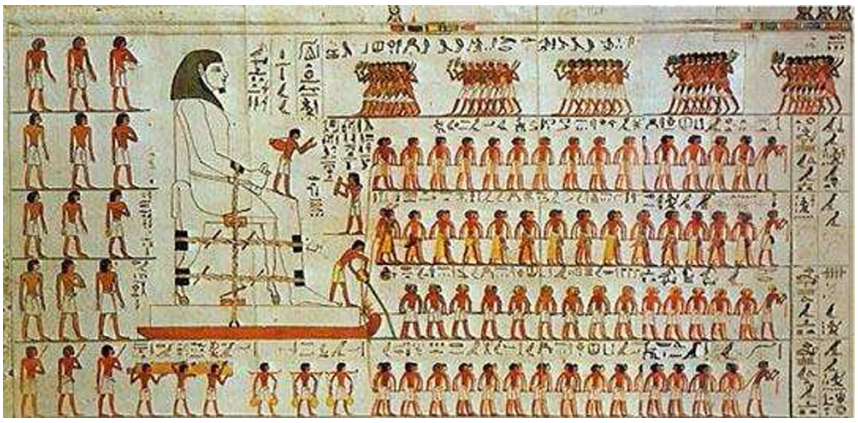

Figure 1.1: Wall painting from 1880 B.C. on the tomb of Djehutihotep. The figure standing at the front of the sled is pouring water onto the sand(from Ref. [27]).

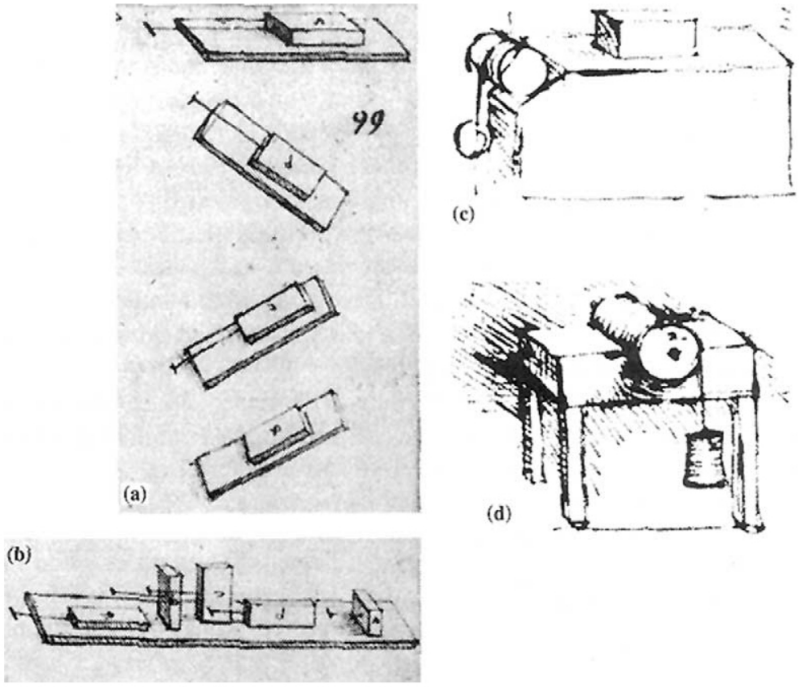

Figure 1.2: Leonardo da Vinci's studies of friction. Sketches from the *Codex Atlanticus* and the *Codex Arundel* showing experiments to determine: (a) the force of friction between horizontal and inclined planes; (b) the influence of the apparent contact area upon the force of friction; (c) the force of friction on a horizontal plane by means of a pulley and (d) the friction torque on a roller and half bearing (from Ref. [30])

1.3 The Standard Model of Dry Friction

From Da Vinci to Amontons-Coulomb Laws

In the 17th century the French physicist Guillaume Amontons rediscovered the da

Vinci's laws of friction after he studied dry sliding between two flat surfaces.

Amontons's conclusions helped to constitute the classic laws of friction. First, the frictional resistance is proportional to the load. Second, and perhaps counter-intuitively, the amount of friction force does not depend on the apparent area of contact of the sliding surfaces: a small block sliding on a surface experiences as much friction as does a large block of the same weight (see Fig. 1.3,1.4).

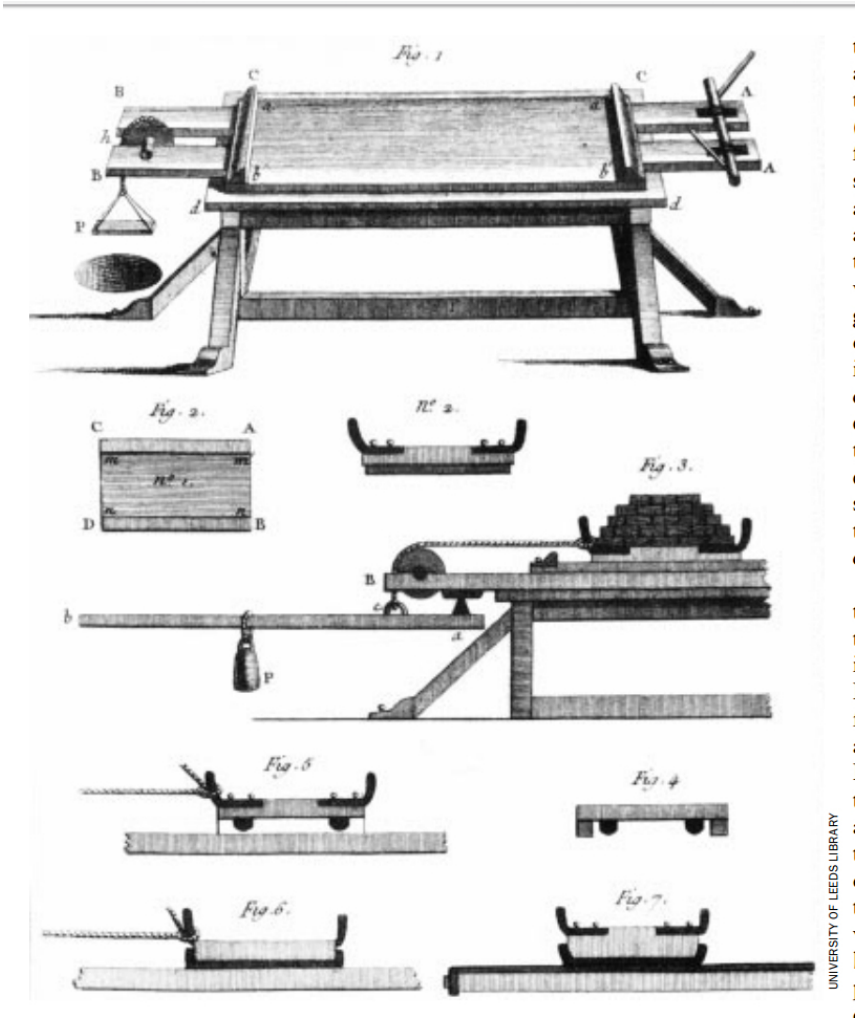

Figure 1.3: EARLY STUDIES OF FRICTION, such as those done in the 18th century by the French physicist Charles-Augustin de Coulomb, helped to define the classical laws of friction and attempted to explain the force in terms of surface roughness, a feature that has now been ruled out as a significant source (from Ref. [30]).

To these rules is added a third law, attributed to the 18th century French physicist Charles-Augustin de Coulomb (better known for his work in electrostatics): the friction force is independent of velocity once motion starts. No matter how fast you push a block,

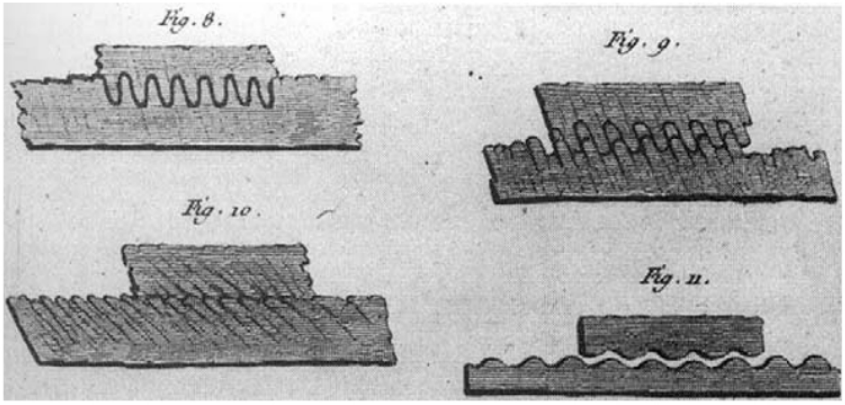

Figure 1.4: Coulomb's representation of rough surfaces, published in 1785 (from Ref. [30])

it will experience nearly the same amount of resistance. Amontons's and Coulomb's classical friction laws have far outlived a variety of attempts to explain them on a fundamental basis in terms of, say, surface roughness or molecular adhesion (attraction between particles in the opposing surfaces).

Consider a solid block-slider lying on a solid flat track (Fig. 1.5); let F be the normal loading force (F may be the weight Mg of the slider) and f the pulling force parallel to the surface of contact of nominal area A_0. Starting from rest, it takes a minimum force

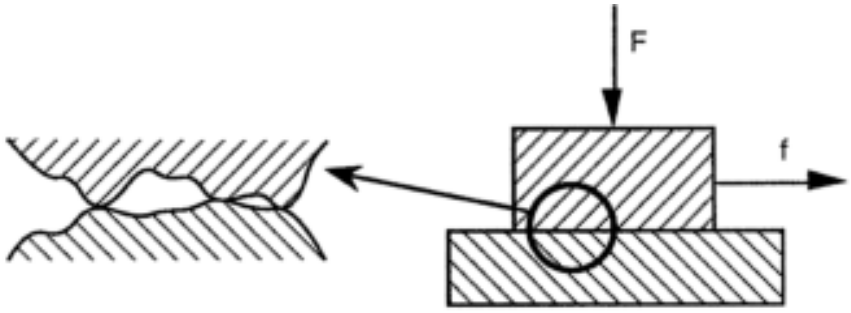

Figure 1.5: Contact between two solid blocks pressed together with a net force F. The pulling force f is parallel to the solid-solid interface. When focusing on the interface the effective contact appears as made of localized patches whose total area is much smaller than the nominal area of contact (from Ref. [33])

$f_s = \mu_s F$ to move the slider: μ_s is the *static* friction coefficient (Fig. 1.6).

When a *steady* sliding motion with velocity v is reached, the friction force $f_d = \mu_d F$: μ_d is the *dynamic* friction coefficient (Fig. 1.6). The classical Amontons-Coulomb's laws state that:

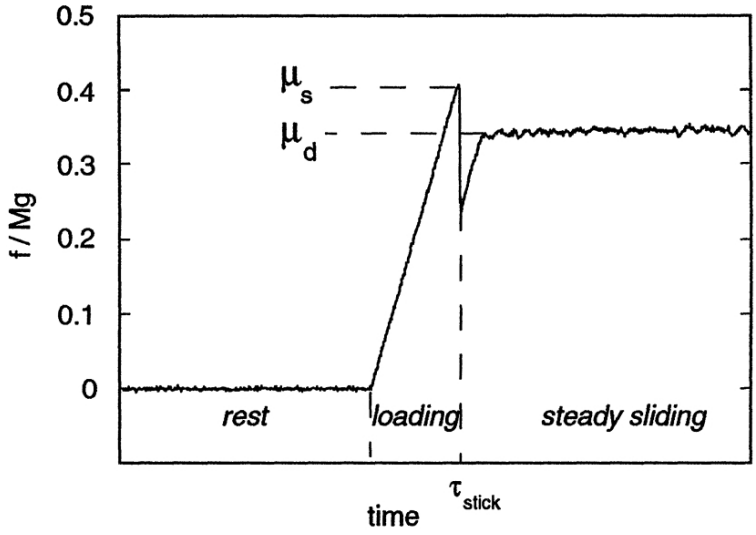

Figure 1.6: Experimental determination of the friction coefficients for paper- paper. At $t = 0$ the slider of mass M is put in contact with the track ; after a while, the pulling force f is increased from zero at constant velocity; after a time $t = \tau_{stick}$, $f = f_s = \mu_s Mg$ and the slider moves. Here, after a transient, the slider achieves steady sliding; the friction force is then $f = f_d = \mu_d Mg < f_s$(from Ref. [33])

- both μ_s and μ_d are independent of F and A_0;
- μ_s and μ_d only depend on the two materials in contact and is usually in the range 0.1-1 ;
- usually $\mu_s > \mu_d$.

1.3.1 The microscopic approach of Bowden & Tabor

A further advance in our understanding of dry friction, in the middle of the twentieth century is bound to two names: Bowden and Tabor [31]. They were the first to advise the importance of the roughness of the surfaces of the bodies in contact [32]. In 1949, Bowden and Tabor proposed a concept which suggested that although independent of friction with the apparent macroscopic contact area A_0, is in fact proportional to the true and *effective* contact area A_{eff} which they called asperities or junctions. That is, the microscopic irregularities of the surfaces touch and push into one another and the area of these contacting regions (Fig. 1.7) is directly proportional to the friction force. Also, they suggested that the origin of sliding friction between clean, metallic surfaces is explained through the formation and shearing of these junctions. According to this understanding, the coefficient

of friction is approximately equal to the ratio of critical shear stress to hardness and must be around 1/6 in isotropic, plastic materials. For many non-lubricated metallic pairings (e.g. steel with steel, steel with bronze, steel with iron, etc.), the coefficient of friction actually does have a value on the order of $\mu \sim 0.16$. The works of Bowden and Tabor triggered an entirely new line of theory of contact mechanics regarding rough surfaces. As pioneering work in this subject we must mention the works of Archard (1957) [34], who concluded that the contact area between rough elastic surfaces is approximately proportional to the normal force. Further important contributions were made by Greenwood and Williamson (1966) [35], Bush (1975), and Persson (2002) [36]. The main result of these examinations is that the real contact areas of rough surfaces are approximately proportional to the normal force, while the conditions in individual micro-contacts (pressure, size of micro-contact) depend only weakly on the normal force.

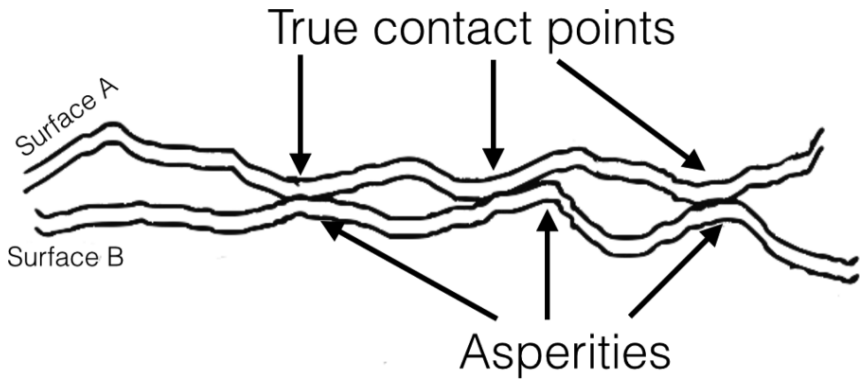

Figure 1.7: Contact area asperity between two surfaces

1.4 Experimental Techniques

The current experimental techniques, capable of study the frictional force that results when islands of atoms, or mono- or bi layers slide over a crystalline substrate, have been opened a new research field involving atomic length scales, called *nanotribology*. The most important result of the experiments is that the atomic scale friction turns out to be viscous, i.e., the friction force is proportional to velocity [37] [20]. In this scale, the vibrations of the layer (phonons) and the electronic substrate excitations (drag of the charge density) are two potentials sources of energy dissipation [38, 39], which is translate as frictional force. However, there is no direct experimental evidence in favor of one or

other of these mechanisms. Electronic friction is, in general, always present, be an atom that slides or a chain. It can be modeled as $m\gamma v$ (where m is the mass of the atoms, γ the electronic friction coefficient and v the sliding velocity) for each of sliding atom, regardless of their number. But if more than one atom is present, it is possible to redirect the sliding energy (of the center of mass) into the system (internal vibrations), due to the interaction (non-linear) with the substrate, which gives rise to the so called phononic friction.

In the last few decades, however, the field of nanotribology was established by introducing new experimental tools, which made the nanometer and atomic scales accessible to tribologists [40, 41, 42, 43]. One of the basic ideas of nanotribology is that for a better understanding of friction in macroscopic systems, the frictional behavior of a single-asperity contact should be investigated first. It is the hope that once the atomic scale manifestations of friction at such a nanometer-sized single asperity have been clarified, macroscopic friction could be explained with the help of statistics.

Table 1.1: Comparison of typical operating parameters in SFA, STM, and AFM/FFM used for micro/nanotribology studies, from Ref. [40]

Operating parameter	SFA	STM	AFM/FFM
Radius of mating surface/tip	10 mm	5-100 nm	5-100 nm
Radius of contact area	10-40 μm	N/A	0.05-0.5 nm
Normal load	10-100 mN	N/A	< 0.1-500 nN
Sliding velocity	0.001-100 μm/s	0.02-200 μm/s (scan size $\sim$ 1 nm x 1 nm to 125 μm x 125 μm; scan rate < 1-122 Hz)	0.02-200 μm/s (scan size $\sim$ 1 nm x 1 nm to 125 μm x 125 μm; scan rate < 1-122 Hz)
Sample limitations	Typically atomically-smooth, optically transparent mica; opaque ceramic, smooth surfaces can also be used	Electrically-conducting samples	None

The emergence and proliferation of proximate probes: as the surface force apparatus (SFA), the scanning tunneling microscopes (STM), atomic force and friction force microscopes (AFM and FFM), and of computational techniques for simulating tip-surface interactions and interfacial properties, have led to the appearance of the new field of nanotribology, which pertains to experimental and theoretical investigations of interfacial processes on scales ranging from the atomic —and molecular— to the microscope, oc-

curring during adhesion, friction, scratching, wear, indentation, and thin-film lubrication at sliding surfaces [44, 45]. Typical operating parameters are compared in Table 1.1.

1.4.1 Surface Force Apparatus (SFA)

The SFA was developed in 1968 and is commonly employed to study both static and dynamic properties of molecular thin films sandwiched between two molecular smooth surfaces. Consists in a block which is pressed against a surface on which exists a lubricating film (Fig. 1.8). The material used for the block and the table is mica, it can be highly polished. In this instrument, the regulation of normal force **F** controls the thickness of the lubricant D allowing to achieve a very thin layer of lubricant. Many researches with the ASF have shown that the type of structure formed between two surfaces determines the friction behavior.

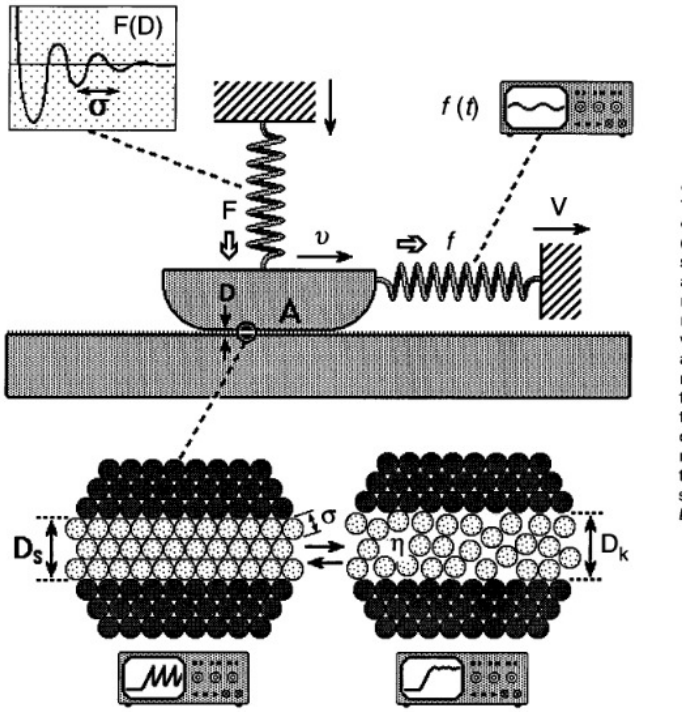

Figure 1.8: Illustration of the principle of the surface-force apparatus (SFA) for measuring the normal forces, **F**, and friction of shear forces **f** , between two smooth surfaces of area A, separated by a thin liquid film of thickness D. An optical interference technique allows the shapes of the surfaces and their separation, D, to be accurately monitored during force and friction measurements (from Ref. [44]).

1.4.2 Scanning Tunneling Microscopes (STM)

The Scanning tunneling microscope was invented by Gerd Binnig and Heinrich Rohrer of IBM's Zurich in 1981 and was the first instrument capable of generating actual images of surfaces with atomic resolution. In 1986 its inventors won the Nobel Prize in Physics [46]. The microscope allows to get atomic resolution of electrically conductive surfaces and has been used to clean surfaces pictures as well as of lubricant molecules [45]. According to Fig. 1.9, the STM is composed of a thin needle coupled to a piezoelectric crystal. This crystal has the ability to generate voltage in response to mechanical pressure. Thus, a potential difference is applied between the needle and the material analyzed. When the tip is placed very close to the sample surface in nanometer-scale approach, the sample surface of the electrons begin to tunnel to the tip of the needle and vice-versa, depending on the applied voltage polarity. When this happens, the tunneled electrons emit a small electrical current (tunneling current). By measuring this electric current, we obtain a topographic image of the surface with an atomic resolution.

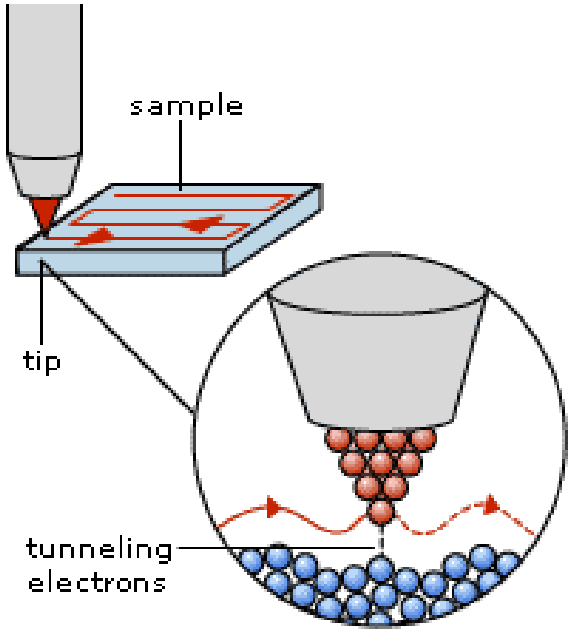

Figure 1.9: Diagram of the Scanning Tunneling Microscope

1.4.3 Atomic Force and Friction Force Microscopes (AFM/FFM)

From a modification of the scanning tunneling microscope (STM), combined with a Stylus profilometer (instrument to measure the roughness on a microscopic scale) Binnig, Quate, and Gerber [47], developed the AFM in 1986. The experimental set-up of an AFM/FFM is shown in Fig. 1.10; it is based on the so-called laser beam deflection method. Cantilever deflection (i.e. normal force) and torsion (friction) of the cantilever are measured simultaneously by detecting the lateral and vertical deflections of a laser beam while the sample is scanned in the x–y-plane. The laser beam deflection is determined using a four-quadrant photo diode: if A, B, C and D are proportional to the intensity of the incident light of the corresponding quadrant, the signal (A + B)-(C + D) is a measure for the deflection and (A +C)-(B + D) a measure for the torsion of the cantilever. A schematic of the feedback system is shown by solid lines. The actual deflection signal of the photo diode is compared with the set point chosen by the experimentalist. The resulting error signal is fed into the PID controller ('PID' stands for a feedback electronics that uses a proportional, an integral, and a differential control part), which moves the z-position of the scanner in order to minimize the deflection signal. Thanks to the FFM measure-

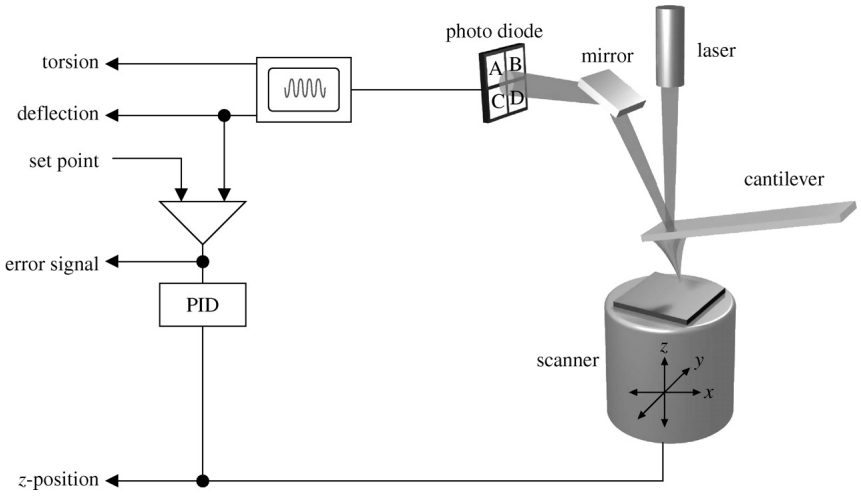

Figure 1.10: Experimental set-up of an AFM/FFM based on the laser beam deflection method (from Ref. [41]).

ment, it was revealed t,0hat the friction laws for a single asperity are different from the macroscopic friction laws. The main result, confirmed by several experiments is that the frictional force at the nanoscale shows a sawtooth behavior, often known as atomic *stick-slip* [37]. This phenomenon can be reproduced by means of models of classical

mechanics [13, 14, 48, 49, 50].

1.4.4 Quartz Crystal Microbalance (QCM)

The Quartz Crystal Microbalance (QCM) (Fig. 1.11) is an instrument that operates on a time scale short enough to detect phonons, whose lifetimes are typically no longer than a few tens of nanoseconds [2]. It has been in use for microweighing purposes and other applications, and modified to study sliding friction of adsorbed layers on metal surfaces in the mid 1980's by Widom and Krim [51]. It works by oscillating a single crystal of quartz, since this material has very little internal dissipation (or friction). As a result it oscillates at an extremely sharp resonance frequency. The oscillations are driven by applying a voltage to thin metal electrodes that are deposited on the surface of the quartz in a manner that produces a crystalline texture. Materials are chemisorbed onto metal electrodes that are grown in ultrahigh vacuum (UHV) conditions onto microbalance. The extra mass of the adsorbed layer lowers the resonance frequency of the microbalance, and the resonance is broadened by any frictional energy dissipation due to relative motion of the adsorbed layer and the microbalance. Changes in the vibrational properties of the quartz indicate how much the deposited layer slips over the substrate. By simultaneously measuring the shift in frequency and the broadening of the resonance, the sliding friction of the layer with respect to the metal substrate can be deduced. The friction can be measured only if it is sufficiently low so as to result in significant sliding. The QCM can, therefore, measure friction between the electrode and a few layers of the chemisorbed material, and provide slip times and interfacial friction coefficients [52].

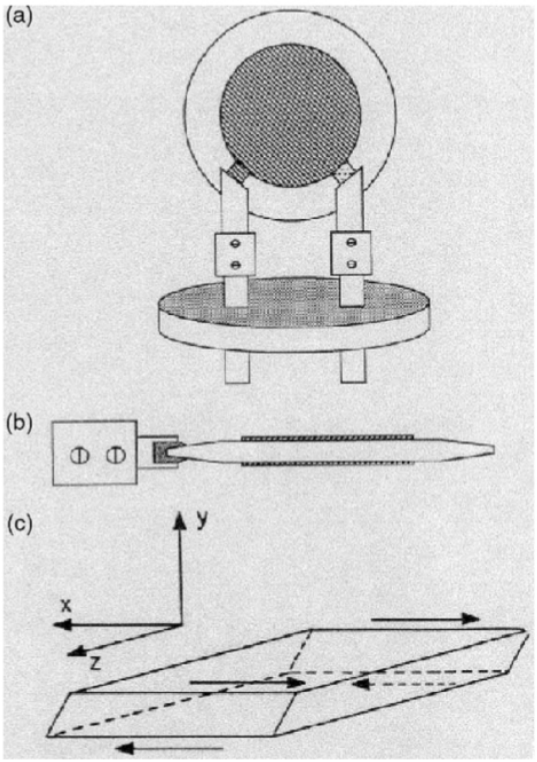

Figure 1.11: Front (a) and side (b) views of a QCM. The shaded regions represent metal electrodes that are evaporated onto the major surfaces of the microbalance. Molecularly thin solid or liquid films adsorbed onto the surface of these electrodes (which are parallel to the x–z plane) depicted in (c) may exhibit measurable slippage at the electrode-film interface in response to the transverse shear oscillatory motion of the microbalance. The experiment is not unlike pulling a tablecloth out from under a table setting, whereby the degree of slippage is deter- mined by the friction at the interface between the dishes (i.e. the adsorbed film material) and the tablecloth (i.e. the surface of the electrode)(from Ref. [2]).

Chapter 2

Theoretical Foundations

A large variety of theoretical approaches have been adopted to study processes at surfaces from a microscopic point of view [20]. The key goal of these approaches is to explain the experimental findings and to predict new phenomena. In this regard, there are two ways to approach the problem: trying to analyze atomic processes and structures in great detail and keeping a close quantitative relation to real systems and experiments, or we can go for "simple (minimalist) models", based on simplified interatomic interactions and focus only on the most relevant degrees of freedom of the system, trying to retain the most important features. The advantage of the second approach is that they are computationally cheap and simple enough to enable us to work out the general mechanisms of the problem, and to provide a deeper physical understanding of the processes at play. These models can explain phenomena of high complexity and allowed to make predictions which were later verified experimentally.

2.1 Prandtl-Tomlinson Model

The development of experimental methods to investigate friction processes at the atomic scale with numerical simulation methods announced a dramatic increase in the number of studies in the area of friction between solids at the atomic scale.

One of the main results, confirmed by several experiments [53, 54], is that the friction force on the nanometer scale exhibits a saw-tooth behavior, commonly known as "stick-slip" motion. This observation can be theoretically reproduced within classical mechanics using the Prandtl-Tomlinson model [14].

Over many years, this model has been referred as the “Tomlinson model" even though the paper by Tomlinson did not contain it. In fact, it was Ludwing Prandtl who suggested in 1928 a simple model for describing plastic deformation in crystals [13]. His contributions were more associated with fluid mechanics [55], mechanics of plastic deformations, friction, and fracture mechanics [56]. In order to correct this historical error, in 2003 Müser, Urbakh, and Robbins, published a fundamental paper [57] in which the mentioned model was termed “Prandtl-Tomlinson Model" [58]. Indeed, the Prandtl-Tomlinson (PT) model has received some renewed attention, as can be seen for example in modeling the aging effect on friction at the atomistic scale [59]. On the other side, Makkonen [3], using a phenomenological thermodynamic approach, connected microscopic quantities obtained by means of AFM, like the adhesion surface energy, with the macroscopic dry friction coefficient. Although the approach seems very promising in predicting real materials coefficients, it does not provide a microscopic explanation of friction.

The model can explain the occurrence of static and kinetic friction, the origin of the *stick-slip* behavior observed in the experiments and the transition to sliding states. It has been successfully used to describe the movement of the tip and to model the scanning process in AFM [60, 61, 62]. Here, we illustrate the properties of this model and its extraordinary versatility to capture the nonlinear nature of frictional dynamics. Consider the Prandtl-Tomlinson model in one dimension and at temperature $T = 0$. A cantilever tip of mass m interacts with the surface via a periodic potential V_{TS} and is attached by a spring of elastic constant K to a support (cantilever) moving at constant velocity v_c along the x direction (see the sketch in Fig. 2.1).

For the 1D case we choose V_{TS} of the form:

$$V_{TS}(x) = U_0[1 - cos(2\pi x/a)] \tag{2.1}$$

where a is the lattice constant of the substrate. The elastic interaction between the tip and the support is

$$V_{el}(x) = \frac{1}{2}k(x - x_s)^2 \tag{2.2}$$

where the support position x_s is

$$x_s = v_c t \tag{2.3}$$

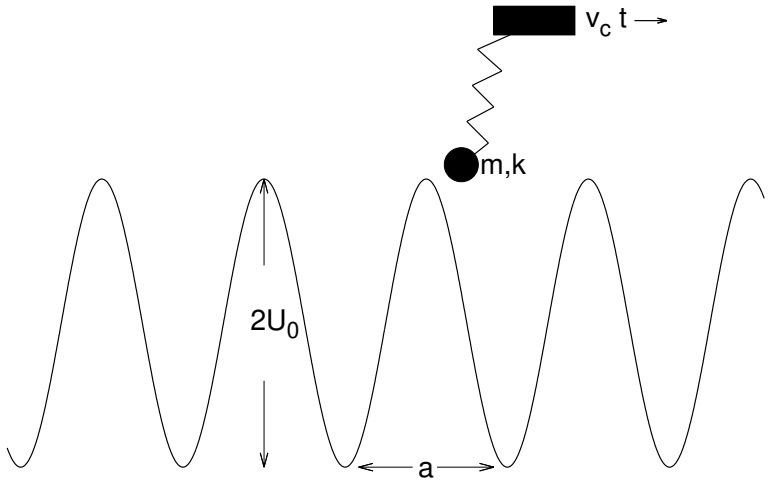

Figure 2.1: Sketch of the 1D Prandtl-Tomlinson model for atomistic friction. The cantilever tip of mass m and constant k is moving at constant velocity v_c. The surface is represented as a potential with corrugation U_0 and period a

It is assumed that the tip is a point-like object, representing the average over many atoms of the real tip-surface contact. Energy dissipation in this model is introduced by adding a damping term proportional to the tip velocity in the equation of motion. Thus, the equation of motion in 1D becomes

$$\boxed{m\ddot{x} + m\eta\dot{x} = -\frac{2\pi U_0}{a}\sin(\frac{2\pi x}{a}) - k(x - v_c t)} \tag{2.4}$$

The solution of Eq. 2.4 is periodic, with period na/v_c [63]:

$$x(t + na/v_c) = x(t) + na, \qquad \text{for} \quad \text{integer} \quad \text{n.} \tag{2.5}$$

Typically $n = 1$ for not too small η, while in the strongly underdamped regime the periodicity of the solution can be an integer multiple of the lattice constant. All energy dissipation during sliding —whether it is due to phonons or due to electronic excitations— is considered by a simple damping term that is proportional to the sliding velocity. This simplification of the atomic-scale energy dissipation process is justified by the assumption that there is no energy dissipation if the tip sticks ($\dot{x} \approx 0$), but energy dissipation will occur as soon as the tip moves [64, 65]. The damping η is often an unknown parameter

in experiments and thus one has to adopt an *ad hoc* choice. Usually a critical damping, $\eta = 2\sqrt{k/m}$ [62] is assumed in order to reduce the oscillations of the tip and to avoid multiple jumps. The underdamped regime is, however, characterized by a very complex dynamical behavior [63]. The character of the motion in the Prandtl-Tomlinson model crucially depends on the interplay between the tip-substrate potential (Eq. 2.1) and the elastic potential (Eq. 2.2), or more specifically on the value of the cantilever stiffness k and of the surface corrugation U_0. The main mechanism of energy dissipation in the model is determined by these elastic instabilities, and therefore we expect a more pronounced contribution to kinetic friction in the stick-slip regime. The $lateral force F_x$ to move the tip in the x direction can be calculated from

$$F_x = k(v_c t - x) \tag{2.6}$$

A typical behavior of the position, velocity and the lateral force of the tip, obtained by solving Eq. 2.4 numerically is shown in Fig. 2.2, 2.3 and 2.4 for two values of U_0, one below and the other above the threshold $U_0 = 1$, when, the behavior goes from being sliding to $stick - slip$.

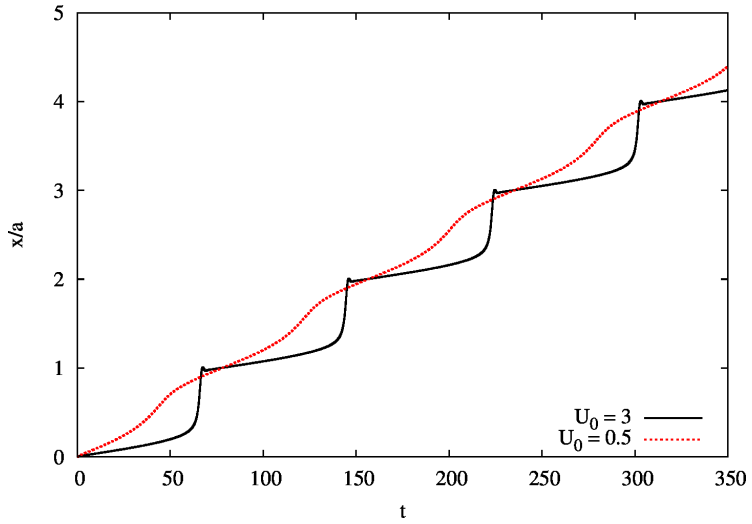

Figure 2.2: Time behavior of the tip coordinate (rescaled to the lattice parameter a), for two values of the reduced corrugation: $U_0 = 0.5$ (below the threshold) and $U_0 = 3$ (above the threshold). While the tip coordinate slides continuously and the lateral force is smooth for $U_0 = 0.5$, stick-slip occurs for $U_0 = 3$, and the tip velocity has sharp peaks corresponding to the slip events. The scanning velocity used in the simulations is $v_c = 0.08$ and the damping is assumed to be critical (η = 2). All quantities are in dimensionless units.

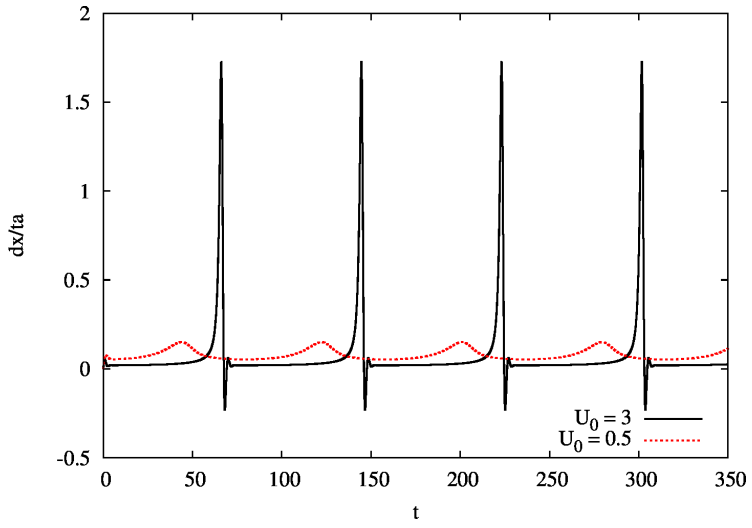

Figure 2.3: Time behavior of the tip velocity for the same conditions as Fig. 2.2.

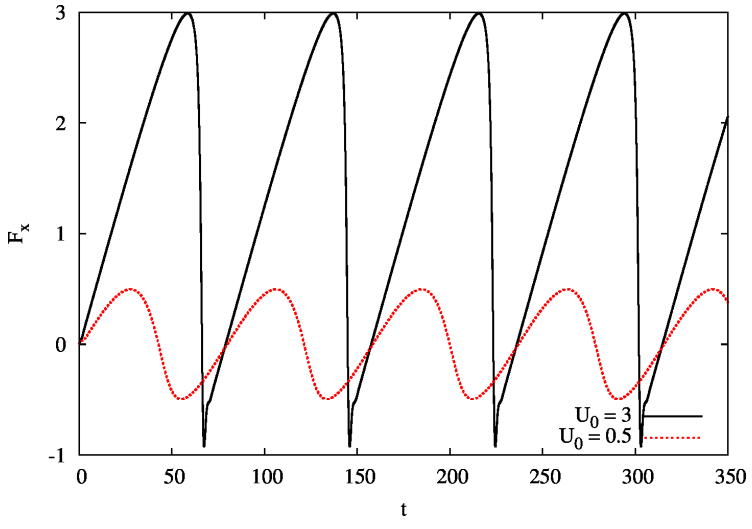

Figure 2.4: Time behavior of the lateral force for the same conditions as Fig. 2.2.

As can be seen in Fig. 2.5 and 2.6, the dynamics of the Prandtl-Tomlinson model is very sensitive to the choice of the damping: when η = 0 there are many oscillations with different frequencies. Whereas in the damped case, the behavior is smoother. The parameter U_0 is which regulates the transition between the sliding motion and stick-slip and thus between high and low friction.

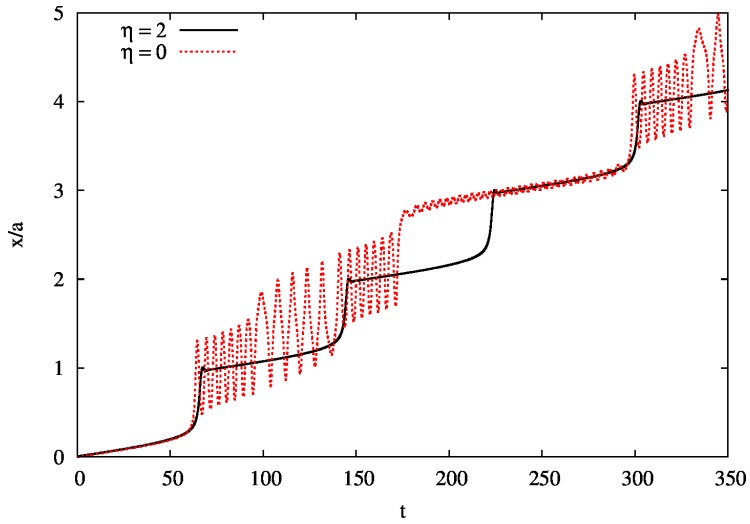

Figure 2.5: Comparison of the tip coordinate (rescaled to the lattice parameter a) for the undamped and the critically damped case, for $U_0 = 3$. The cantilever scanning velocity is $v_c = 0.08$. All quantities are in dimensionless units.

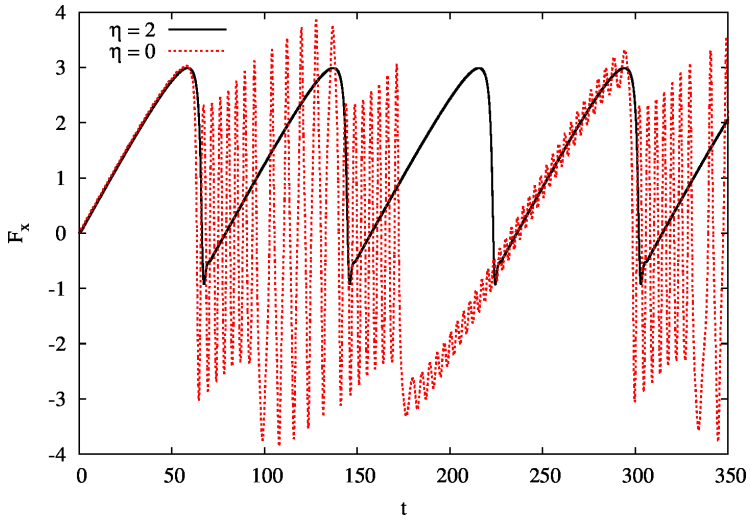

Figure 2.6: Comparison of the lateral force (rescaled to the lattice parameter a) for the undamped and the critically damped case, for $U_0 = 3$. The cantilever scanning velocity is $v_c = 0.08$. All quantities are in dimensionless units.

A work carried out by Socoliuc [66] using this model (Fig. 2.7) shows the comparison

between experimental results for different loads values compared to simulations of Eq. 2.6 for different values of U_0 (effective corrugation). The qualitative behavior is the same, and interestingly, the behavior of the stick-slip movement and its hysteresis becomes less evident as the load U_0 decreases. These results are very significant, because they suggest a way to control the friction in nanoscale without the use of lubricants, emphasize the strength of the Prandtl-Tomlinson model in the description of dynamic friction.

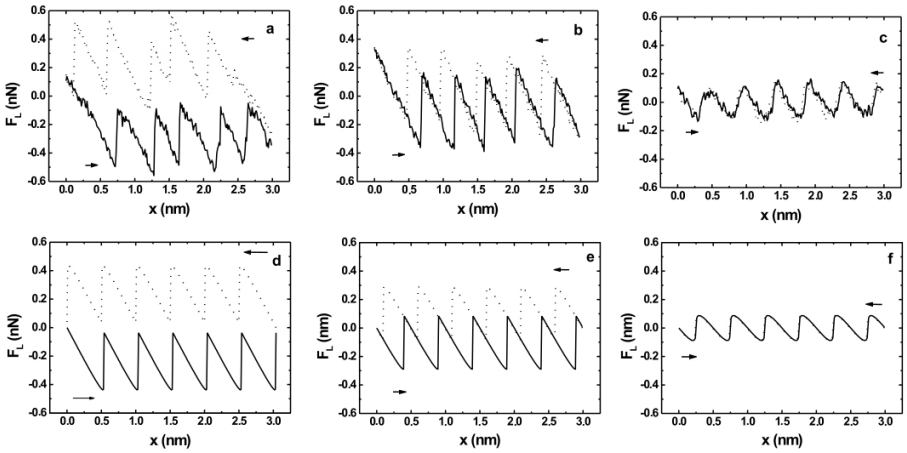

Figure 2.7: Lateral force as a function of the tip position, as obtained by AFM experiments on NaCl(a-c) and by simulations of the Prandtl-Tomlinson model (d-f). The normal applied loads in the experiments are $F_{load} = 4.7nN$ (a), $F_{load} = 3.3$ (b) and $F_{load} = -0.47$ (c), while the values of U_0 are $U_0 = 5$ (d), $U_0 = 3$ (e) and $U_0 = 1$ (f). Notice the transition from stick-slip to sliding by decreasing the load in the experiments and by decreasing the effective corrugation U_0 in the simulations [66].

2.1.1 Velocity Dependence of Friction

As it was already mentioned in the introduction, the empirical laws of macroscopic friction cannot always be applied at the atomic level. One of them is the dependence of friction with velocity. In this respect, several models and a varied of conclusions have emerged and still controversy continues.

In the original experiments of Mate et al. [53] the authors observed that the frictional force on a tungsten tip sliding on the basal plane of graphite for small loads shows little dependence on velocity for scanning velocities up to $400\,\mathrm{nm/s}$. On Zworner (1998) [64] paper, the authors show the results of the velocity dependence of the friction at the contact

point between the tip and the substrate (Fig.2.8). The experimental results were obtained using a frictional force microscope. It was found that the frictional forces are independent of the sliding velocity, even in the nanometer scale for all sliding speeds performed, as long as the sliding movement of the tip be faster than the sliding velocity.A similar behavior has also been reported in the work of Zworner et al. [64] for velocities up to several $\mu m/s$, where friction on different carbon structures has been studied. The authors of [64] claim that a 1D Prandtl-Tomlinson model at $T = 0$ can reproduce a velocity independent friction force for scanning velocities up to $\sim 1\,\mu\mathrm{m/s}$, while giving rise to linear increase of friction for higher velocities. They conclude that F_{fric} is nearly constant in this range of low velocities. With increasing sliding velocity, the frictional force is just proportional to v_c owing to the viscous damping $F_{fric} \sim \gamma x v_c$ which is indicated by the dashed line.

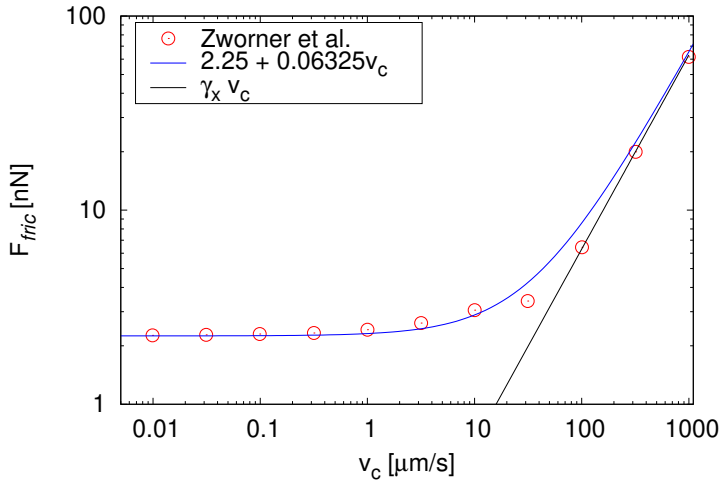

Figure 2.8: Data extracted from Zworner *et al.* [64] showing the frictional force (F_{fric}) as a function of the sliding velocity (v_c), along with the analytic expressions of the two limiting regimes.

Other works claim a logarithmic increase in the friction force with velocity, attributed to thermal activation [67, 71, 37, 72, 73, 74, 75]. Fusco and Fasolino [20] have shown that an appreciable velocity dependence of the friction force, for small scanning velocities (from $1\,\mathrm{nm/s}$ to $1\,\mu\mathrm{m/s}$), is inherent to the Prandtl-Tomlinson model, having the form of a power-law $F_{fric} - F_0 \propto v_c^{2/3}$. (Figure 2.9)

Depending on the investigated systems and/or models, on the simulation techniques and/or conditions, different and somewhat contradictory results have been found on this subject [20], even when using the same model.

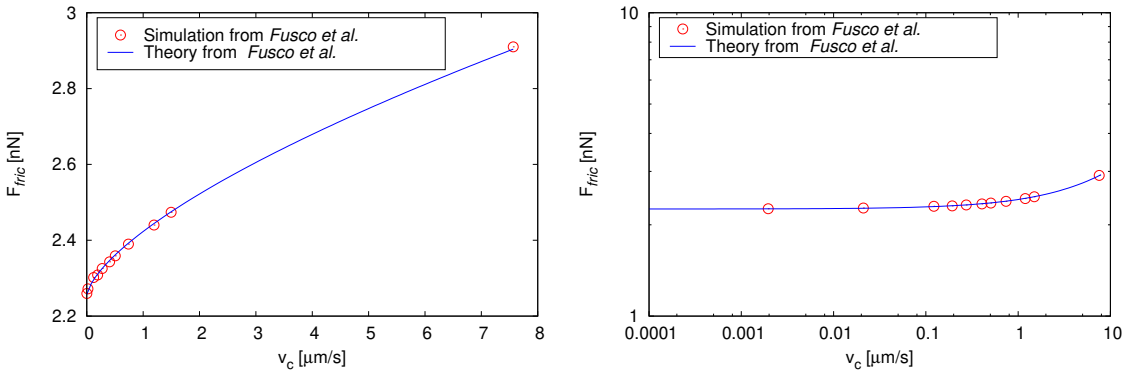

Figure 2.9: Data extracted from Fusco and Fasolino [20] showing the friction force (F_{fric}) as a function of the sliding velocity (v_c), plotted on a linear (top) and on a log-log scale(bottom), in the same way it was presented in the original article.

2.2 The Frenkel-Kontorova Model

The Frenkel-Kontorova model is one of the most simplest and rich models in classical mechanics. Involves a system shown in Fig. 2.10 where a one-dimensional chain of atoms connected by springs of average length a interact with a harmonic potential in period b [15]. The model was introduced at first to study dislocation in crystals, but it soon proved useful in studying the mechanism of friction such as the origin of static friction and effect of structural commensurability. The simplicity of the model, due to the assumptions of the harmonic interatomic force and sinusoidal on-site (substrate) potential, as well as its surprising capability to describe a broad spectrum of nonlinear, physically important phenomena, such as propagation of charge – density waves, the dynamics of absorbed layers of atoms on crystal surfaces, commensurable–incommensurable phase transitions, domain walls in magnetically ordered structures, etc., have attracted a great deal of attention from physicists working in solid state physics and nonlinear physics [76]. One of the important features which can explain why the FK model has attracted much attention in different branches of solid state physics is the fact that in the continuum-limit approximation the model reduces to the exactly integrable sine-Gordon (SG) equation which possesses nice properties and allows exact solutions describing different types of nonlinear waves and their interaction. In particular, the SG equation gives us an example of a fundamental nonlinear model for which we know almost everything about the dynamics of nonlinear excitations. As is known, the SG system describes simultaneously three different types of elementary excitations, namely phonons, kinks (topological solitons), and

breathers (dynamical solitons), whose dynamics determines the general behavior of the system as a whole. And, although the FK model is inherently discrete and not exactly integrable, one may get deep physical insights and significantly simplify the understanding of its nonlinear dynamics using the language of the SG quasi-particles as weakly interacting nonlinear excitations. Discreteness of the FK model manifests itself in such a phenomenon as the effective periodic potential, known as the Peierls—Nabarro relief, affecting the quasi-particle motion.

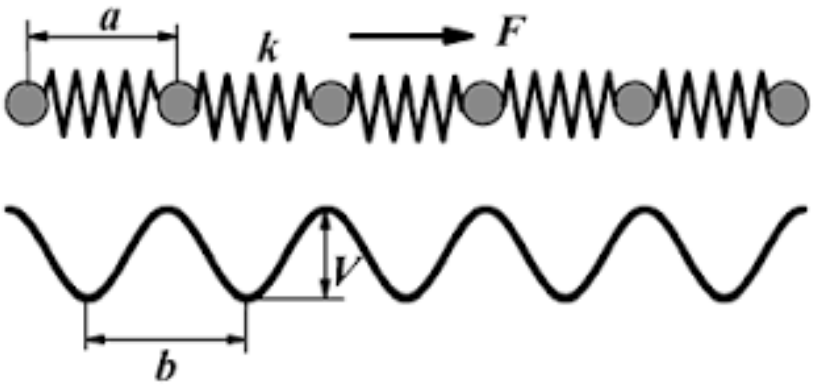

Figure 2.10: Schematic of the Frenkel-Kontorova model.

The dimensionless equation of motion for the atomic chain can be written as

$$\ddot{x}_j + \gamma\dot{x}_j = (x_{j+1} - 2x_j + x_{j-1}) - \lambda sin2\pi x_j + F \tag{2.7}$$

with $j = 1, 2, ..., N$ and x_j is the position of the jth atom, γ denotes the internal damping coefficient in the atomic chain, $\lambda = V/k$ represents a normalized potential strength equal to the magnitude of the sinusoidal potential divided by the spring stiffness k, and F is an external driving force. The contour conditions are:

$$x_{j+N} = x_j + 2\pi M$$

where M is an integer number. This conditions imply that the mean of the particles density $1/c$ is constant:

$$c = 2\pi\frac{M}{N} \tag{2.8}$$

because of the symmetry, c is restricted to $[0, \pi]$. Several studies were carried out using the above equation and friction as the focus, among them: in the super-damped

regime for large N [77, 78, 79], at the limit with damping and external force equal to zero [80]; in the sub-damping regime for small N [81, 82]; in the generalized under-damped regime with large N and c near 0 and π [83]. But the most relevant fundamental work is that of Strunz and Elmer [84]. This work differs only in the fact that c is not restricted to any value in relation to the values studied in [83]. They find that Eq. 2.7 has stable and unstable solutions, describing respectively two types of regular slip states: uniform slip states and non-uniform slip states. Fig. 2.11 shows these states. The force versus velocity characteristic curve shows stable and unstable solutions. Macroscopically, this curve would have linear character of type $F = \gamma v$. However, resonance of the chain of adatoms for certain speeds of sliding results in the formation of phonons and consequently peaks in the characteristic curve

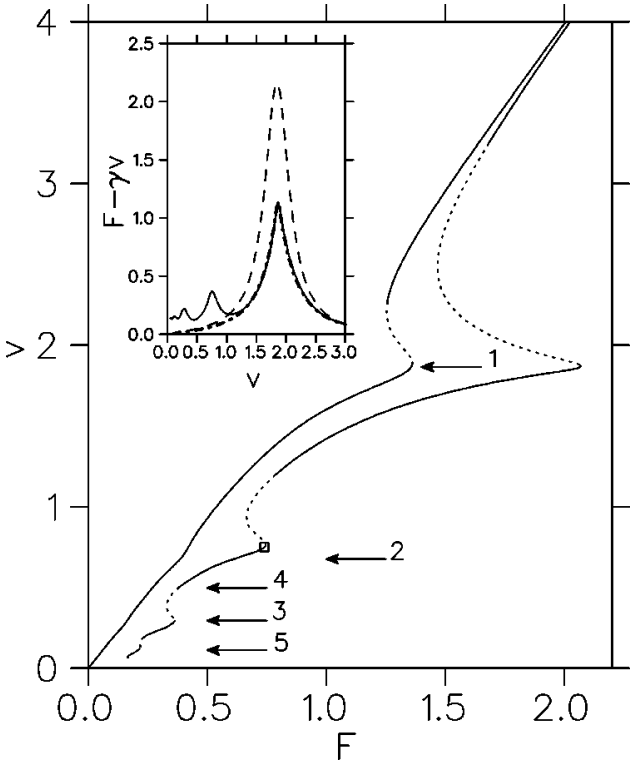

Figure 2.11: Velocity-force characteristic. Solid (dotted) lines indicate stable (unstable) solutions. The smaller graph represents analytic solutions found. Arrows indicate resonant peaks, from Ref. [84].

The model was widely used to answer issues like how the energy dissipates on the substrate, which is the main dissipation channel (electronic or phononic), and how the phononic sliding friction coefficient depends on the corrugation amplitude [85, 86, 87]. In the work of [25], the authors used the FK model of an adsorbate-substrate interface to

calculate the phononic friction coefficient. They investigated the system, for different substrate/adsorbate commensuration ratios in order to address how the phononic friction (and therefore the sliding friction) depends on the commensuration ratio between substrate and adsorbate. And demonstrate that the phononic friction coefficient depends quadratically

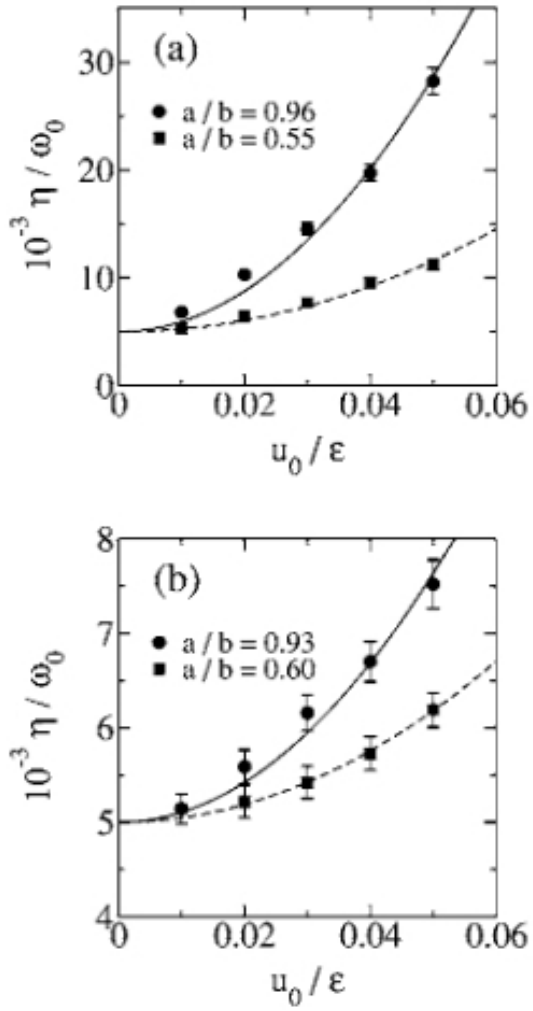

Figure 2.12: Total friction coefficient from different commensuration ratios (from Ref. [25])

on the substrate corrugation amplitude, but is a nontrivial function of the commensuration ratio between substrate and adsorbate (Fig. 2.12).

In reference to this last subject, and from a experimental point of view, a recent work was published [88] where the authors investigate the isotopic role on the dissipative forces acting at the nanoscale in order to overcome the problem of the surface coverage ratio effect on the friction phenomenon.

They discuss the issue of friction between a diamond spherical dome sliding on amor-

phous carbon thin films containing different amounts of deuterium and/or hydrogen that modifies the phonon-only distribution. Being more specific, the experimental results take into account the physical contact under pressure arising between two sliding surfaces in relative motion. They show that the friction coefficient decreases by substituting hydrogen by deuterium atoms. This result is consistent with an energy dissipation vibration local mechanism from a disordered distribution of bond terminators.

Chapter 3

Models and Methods

In this work, in addition to explore the Prandtl-Tomlinson Model to analyze the dependence of the friction with velocity, two one-dimensional models were proposed to represent the interaction between a substrate and a AFM microscope tip. In both cases, the substrate is represented by independent harmonic oscillators. In the first model only two particles are considered and in the second the substrate is represented by a chain of particles. The interaction between the tip and the substrate is a short-range Gaussian type potential. In no case is any type of "ad-hoc" dissipation considered.

3.1 First Model: Energy exchange in a two particles system

The first model consists of two particles: a mass that is thrown to move past another one, which is attached to a spring (Fig. 3.1). The interaction between the particles is nonlinear and short-ranged. For simplicity, the motion is considered in one dimension, but the free particle can overcome the bound one because the interaction potential between them has a finite maximum. This seemingly unreal situation is a simplified model of a particle sliding on top of another, where the transverse movement is not taken into account. The asperity is represented by a single free particle and the substrate by a harmonic oscillator. As shown in Fig. 3.1 the free particle is impelled from a region where it is not affected by the presence of the oscillator, until eventually it interacts with it. This local interaction is repulsive, short ranged, and with a finite maximum; for simplicity a Gaussian is used for the interaction potential.

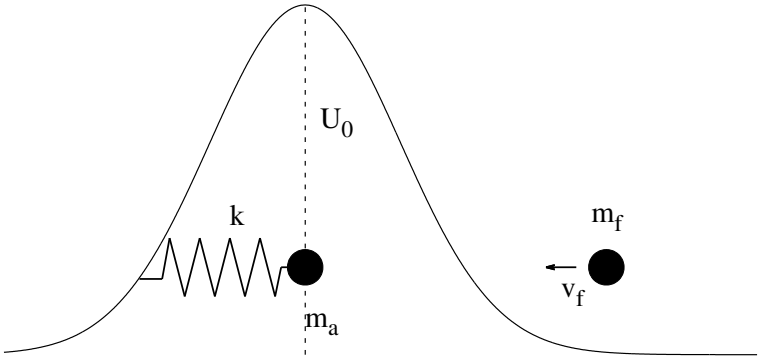

Figure 3.1: Schematic representation of the two particle model.

Therefore the proposed model is represented by the Hamiltonian

$$H = \frac{p_f^2}{2m_f} + \frac{p_a^2}{2m_a} + \frac{1}{2}m_a\omega^2 x_a^2 + U(x_f, x_a) \tag{3.1}$$

where $p_f,\ x_f,\ p_a,\ x_a$ are the momentum and position of the free particle and the oscillator respectively. The masses of the two are unequal and represented by m_f and m_a respectively. The oscillator frequency is $\omega = \sqrt{k/m_a}$, where k is the spring constant. As it was said, the interaction potential $U(|x_f - x_a|)$ is assumed to be a Gaussian with a maximum value U_0, the height of the potential, and a width σ, which characterizes the typical range or length of the interaction. From the Hamiltonian in Eq. (3.1), the following equations of motion are derived:

$$\ddot{x}_f = \left(\frac{2U_0}{m_f\sigma^2}\right)(x_f - x_a)e^{-\frac{(x_f-x_a)^2}{\sigma^2}} \tag{3.2}$$

$$\ddot{x}_a = -\omega^2 x_a - \left(\frac{2U_0}{m_a\sigma^2}\right)(x_f - x_a)e^{-\frac{(x_f-x_a)^2}{\sigma^2}}\ , \tag{3.3}$$

which have five parameters. By defining dimensionless variables $q = x/\sigma$ and $\tau = \sqrt{\frac{U_0}{m_f\sigma^2}}\ t$, and writing the equations of motion in terms of them,

$$\ddot{q}_f = 2(q_f - q_a)e^{-(q_f-q_a)^2} \tag{3.4}$$

$$\ddot{q}_a = -\frac{\Gamma^2}{\mu}q_a - 2\frac{(q_f - q_a)}{\mu}e^{-(q_f-q_a)^2}\ , \tag{3.5}$$

the number of free parameters can be reduced to two: the ratio of the masses of the two objects ($\mu = \frac{m_a}{m_f}$), and a dimensionless oscillator frequency ($\Gamma = \sqrt{\frac{k\sigma^2}{U_0}}$). It is therefore important to understand the dynamics of the system in terms of the relative masses and the frequency of the oscillator, which is addressed in the next section.

Working with Eqs. (3.2) and (3.3), the behavior of the system in terms of those two parameters is characterized. It is worth to notice that the Gaussian potential was chosen for no particular reason except for being simple an short ranged, capturing the essential features of the interaction among the "substrate" and "adsorbate". On the other side, it makes the problem nonlinear with no close analytic solution.

3.2 Second Model: Prandtl-Tomlinson model improved with no ad-hoc dissipation

The second model proposed and studied is an extension of the last model (Fig. 3.2), where m_s, k_s are the masses of the substrate particles and their spring constants; m_t, k_t are the tip mass and spring constant respectively. U_0 is the height of the interaction potential and a_x is the lattice constant. The tip is driven by a support that moves at constant velocity v_c . The substrate is represented by a series of spring-masses, independent between them, but interacting with the tip via a short range Gaussian type potential. To avoid edge effects we modeled the chain as being sufficiently long.

The system is described by the Hamiltonian

$$H = \frac{P^2}{2m_t} + \sum_{i=1}^{N}\frac{p_i^2}{2m_s} + \sum_{i=1}^{N}U(X, x_i) + U(X) + \sum_{i=1}^{N}U(x_{s_i}) \tag{3.6}$$

where X, P and x, p are the tip and substrate coordinates respectively; $U(X, x_i) = U_0 e^{-\frac{(X-x_i)^2}{\sigma^2}}$ is the interaction between the tip and each of the particles of the substrate and N is the number of particles. We choose the value of σ such that the potentials do not

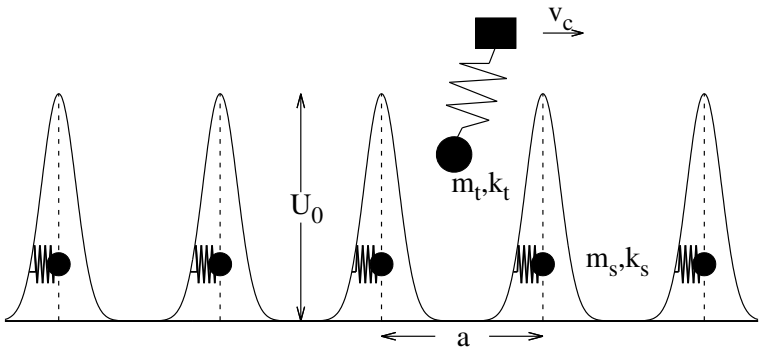

Figure 3.2: Extension of the two particles interaction model to a N-particle model: m_s and k_s are the mass and spring constant of the substrate; m_t , k_t are the tip mass and spring constant respectively. U_0 is the height of the interaction potential and a is the lattice constant. The tip is driven by a support that moves at constant velocity v_c

overlap each other and the tip can interact with each of them separately: $\sigma = a_x/n$, where a_x is the separation between the particles of the substrate and n a constant. $U(X) = \frac{k_t}{2}(X - x_c)^2$ is the elastic interaction between the tip and the cantilever. The support position x_c is $x_c = v_c t$.And $U(x_i) = \frac{k_s}{2}(x_i - x_{0_i})^2$ is the elastic potential of each particle (independent between them). The energy dissipation can be added introducing a damping term proportional to the tip velocity.

This results in the following equation of motion:

$$m_t\ddot{X} = -k_t(X - v_c t) + \frac{2U_0}{\sigma^2}\sum_{i=1}^{N}(X - x_i)e^{-\frac{(X-x_i)^2}{\sigma^2}} \tag{3.7}$$

$$m_s\sum_{i=1}^{N}\ddot{x_i} = -k_s\sum_{i=1}^{N}(x_i - x_{0_i}) - \frac{2U_0}{\sigma^2}\sum_{i=1}^{N}(X - x_i)e^{-\frac{(X-x_i)^2}{\sigma^2}} \tag{3.8}$$

Introducing the dimensionless units $Q = \frac{X}{\sigma}, q = \frac{x}{\sigma}, \tau = \sqrt{\frac{k_t}{m_t}}t, \tilde{U_0} = \frac{2U_0}{k_t\sigma^2}, \tilde{v_c} = \frac{v_c}{\sigma}\sqrt{\frac{m_t}{k_t}}$, the equations 3.7 and 3.8 can be reduced to:

$$\ddot{Q} = -q + \tilde{v_c}\tau + \tilde{U_0}\sum_{i=1}^{N}(Q - q_i)e^{-(q_t - q_{s_i})^2} \tag{3.9}$$

$$\sum_{i=1}^{N}\ddot{q}_i = \frac{\epsilon_1}{\epsilon_2}\sum_{i=1}^{N}(q_i - q_{0_i}) - \epsilon_1\tilde{U_0}\sum_{i=1}^{N}(Q - q_i)e^{-(Q-q_i)^2} \tag{3.10}$$

where $\epsilon_1 = m_t/m_s$ is the ratio of the mass of the tip and the substrate particles (assuming all have the same masses) and $\epsilon_2 = k_t/k_s$ is the ratio of the stiffness of the tip and the substrate.

3.3 Molecular Dynamics

Computer simulations have played an important role in advancing our understanding of tribological processes [90, 40]. They allow controlled numerical experiments where the geometry, sliding conditions, and interactions between atoms can be varied at will to explore their effects on friction, lubrication, and wear. Unlike laboratory experiments, computer simulations enable scientists to follow and analyze the full dynamics of all atoms. Moreover, theorists have no other general approach to analyze processes like friction and wear, because there is no known principle like minimization of free energy that determines the steady state of nonequilibrium systems. Even if there were, simulations would be needed to address the complex systems of interest, just as in many equilibrium problems.

As the equations of motion of an adsorbate on a substrate, can not, in general, be solved analytically, it is necessary to appeal to numerical simulations. The main technical work for this research is the Molecular Dynamics (MD), in which the dynamics is calculated by solving classically the equations of motion of the system [89]; also is an excellent tool to approach the study of the microscopic friction.The technique is described extensively in a number of review articles and books, including Allen [91] and Frenkel and Smit [92]. The basic outline of the method is straightforward. One begins by defining the interaction potentials. These produce forces on the individual particles whose dynamics will be followed, typically atoms or molecules. Next the geometry and

boundary conditions are specified, and initial coordinates and velocities are given to each particle. Then the equations of motion for the particles are integrated numerically, stepping forward in time by discrete steps of size Δt. Quantities such as forces, velocities, work, heat flow, and correlation functions are calculated as functions of time to determine their steady-state values and dynamic fluctuations. The relation between changes in these quantities and the motion of individual molecules is also explored.

In this way, the temporal and spatial evolution of the adsorbate are calculated when interact with the surface atoms. In MD, the form of potential energy is given explicitly as a function of the position of atoms. Although the MD simulations can give very precise results and are able to follow the dynamic details of the system, in most cases are limited to short time scales (in the order of 100 ns) since the typical time interval is very tiny. Several studies using this technique have been made in recent years [18] [24] [21] [25]. There are several ways to solve the equations numerically. Basically, we have to include the stochastic forces on the algorithm used to solve deterministic equations, such as the Verlet and Velocity Verlet algorithm, used in this work.

3.3.1 Verlet Algorithm

The numerical integration of the equations of motion is performed by algorithms based on the finite difference method, in which the integration is divided into small time steps (integration step) [93], Δt, such as Velocity Verlet or Runge-Kutta [91, 92, 94, 95]. One of the most used methods in molecular dynamics to integrate the equations of motion is the Verlet algorithm, which uses the positions and accelerations of atoms at time t and the previous step positions, $r(t - \Delta t)$ to determine the new position at time $t + \Delta t$ as we can see from Eq. 3.11

$$r(t + \Delta t) = 2r(t) - r(t - \Delta t) + \frac{f(t)}{m}\Delta t^2 \tag{3.11}$$

This algorithm can be obtained through expanding in Taylor series, initially forward (Eq. 3.12), and then backwards (Eq. 3.13). Adding the two equations and isolating $r(t + \Delta t)$, we get the Eq. 3.11 (9)

$$r(t + \Delta t) = r(t) + v(t)\Delta t + \frac{1}{2}\frac{f(t)}{m}\Delta t^2 + ... \tag{3.12}$$

$$r(t - \Delta t) = r(t) - v(t)\Delta t + \frac{1}{2}\frac{f(t)}{m}\Delta t^2 - ... \tag{3.13}$$

The velocity is given by

$$v(t) = \frac{r(t + \Delta t) - r(t - \Delta t)}{2\Delta t} \tag{3.14}$$

3.3.2 Velocity Verlet Algorithm

In our simulations we have employed the velocity Verlet algorithm, which, at variance with the Runge-Kutta, is a symplectic algorithm (i.e. it retains many dynamical properties of the phase space that the exact trajectories are known to exhibit), and thus it is more robust and stable. The velocity Verlet algorithm computes the particle velocity $v(t + \Delta t)$ and the position $r(t + \Delta t)$ at time $t + \Delta t$as follows:

$$r(t + \Delta t) = r(t) + v(t)\Delta(t) + \frac{F(t)\Delta t^2}{2m} \tag{3.15}$$

$$v(t + \Delta t) = v(t) + \frac{(F(t) + F(t + \Delta t))\Delta t}{2m} \tag{3.16}$$

In the equations above, $F(t)$ is the force at time t acting on the particle, which depends only on the position $x(t)$. The algorithm is self starting.

Chapter 4

Results and Discussions

This chapter is divided into three sections: the first one corresponds to the velocity-friction dependence in the Prandtl-Tomlinson model [68]. The second section is dedicated to the results of the first [69] model and the third to the results of the second model [70].

4.1 Prandtl-Tomlinson model revisited

Considering the variety of seemingly conflicted results, in this chapter we address this apparent paradox in the Prandtl-Tomlinson model at zero temperature, studying the force-velocity relation for a wide range of velocities not previously presented. Including much more data density for the non trivial regions, we are able to shed light on this problem and at the same time, provide new insight in the use of the paradigmatic Prandtl-Tomlinson model for the secular problem of friction laws.

In this way we can show that depending on how the results are presented, it is possible to arrive to apparently different conclusions. However, taking the whole picture, the results of the different contributions can be reconciled.

In Fig. 4.1 is shown the lateral force F_x; and tip velocity v_t in Fig. 4.2 for different sliding velocities using the model of Prandtl-Tomlinson. The values of the constants for the model are: k = 10 N/m, m = 10^{-10} kg (which gives a natural frequency for the tip, $\sqrt{k/m} \simeq 316$ kHz), and a = 0.3 nm, typical values of AFM experiments [71, 62, 64, 20]. In general, the amplitude used for the corrugation U_0 goes from 0.2 to 2 eV [72], and in the present case we use U_0 = 1 eV. We chose $\gamma = 2\sqrt{k/m}$ in order to have critical damping,

and the time step used for the numerical integration was $\Delta t \simeq 1\,\mathrm{ns}$ [1]. These particular set of parameters were chosen in order to compare our results with those obtained by Zworner *et al.* [64] and Fusco and Fasolino [20].

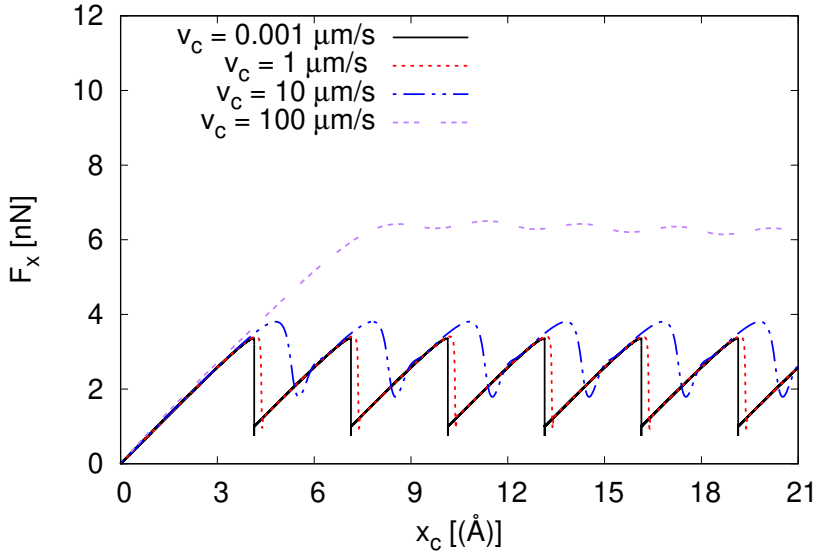

Figure 4.1: Lateral force F_x for different sliding velocities $v_c = 0.001\mu m/s$ to $10\mu m/s$

If to each sliding velocity, we compute the average of the frictional force F_{fric} over many *stick-slip* periods, we obtain the Friction force in function of the sliding velocity of the cantilever.

With the help of the software Engauge Digitizer [96] we recover the data points from the graphics of the mentioned references; in this way we can reproduce the plots of their simulations in the most similar way to the original articles as it was shown on Fig. 2.9

This also allowed us to make graphics along with the results from our own simulations (as shown in Fig. 4.3), so we can compare the three set of data in the different regions.

Our numerical results are extended down to $0.1\,\mathrm{nm/s}$, in order to show that, in principle, all data seems to be consistent. It can be appreciated from the plot in linear scale (Fig. 4.3 left), that this consistency is hard to appreciate, particularly under $1\mu m/s$ where many order of magnitude are condensed. For this reason, the same data has to be presented in a more convenient scale, which is the case of a semi-log scale (Fig. 4.3 right).

[1] The period of oscillation of the cantilever is $20\,\mu\mathrm{s}$ and the maximum simulated speed is $1\,\mathrm{mm/s}$, so that time step is more that 1000 times smaller that the period and at the maximum speed it moves only $1/300$ of the potential length

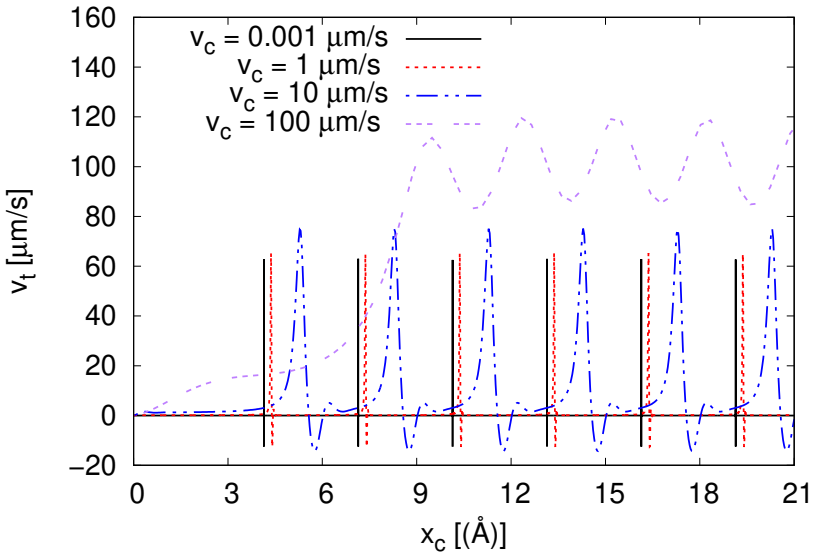

Figure 4.2: Tip velocity dx/dt for different sliding velocities $v_c = 0.001\mu m/s$ to $10\mu m/s$

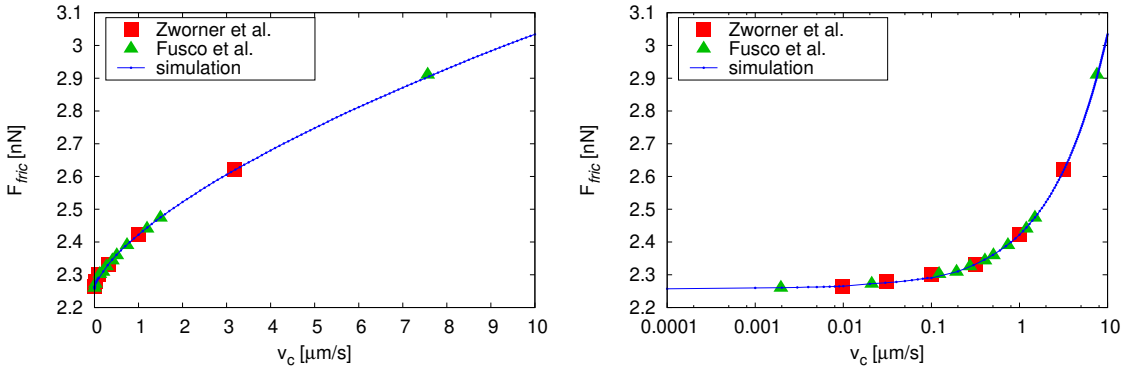

Figure 4.3: Comparison between data from Zworner *et al.* [64], Fusco and Fasolino [20] and from present contribution in semi-log scale.

Zworner *et al.* [64] use a wide range of velocities (from $10^{-2}\ \mu\mathrm{m/s}$ to $10^{3}\ \mu\mathrm{m/s}$) so it is interesting to analyze in detail the results on different regions.

In their work, the authors concluded that the model exhibits two limiting behaviors for the resulting frictional force (Fig. 2.8): a velocity independent regime at low velocities, below $1\ \mu\mathrm{m/s}$ and a viscous linear regime for velocities $\geq 100\ \mu\mathrm{m/s}$. We can see in Fig. 4.4 that these two limiting cases —and particularly the combination of both— can give an approximated description of the Prandtl-Tomlinson model results in the wide region of velocities displayed. However, one has to be aware that the log-log scale used to present the data might hide possible departures from such behavior, providing an over-

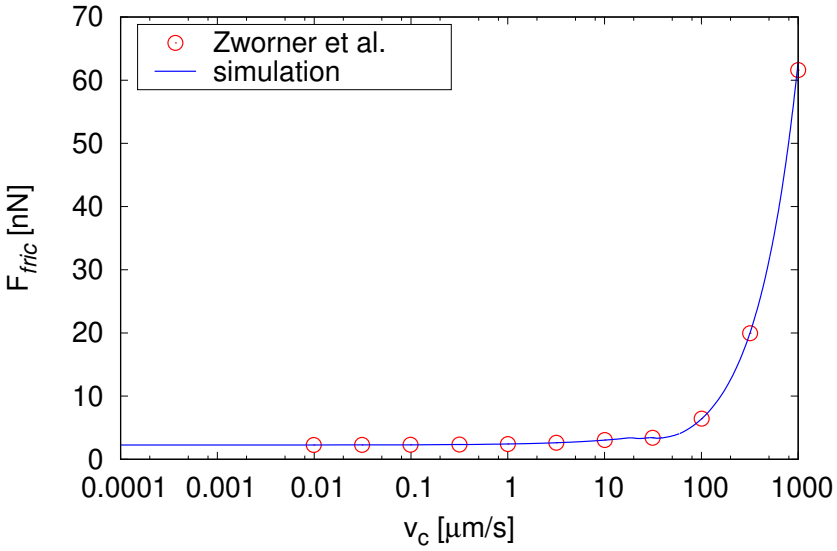

Figure 4.4: F_{fric} as a function of v_c in semi-log scale; comparison between Zworner *et al.* [64] simulations and present numerical results with the athermal Prandtl-Tomlinson model.

simplification of the otherwise rich features of the Prandtl-Tomlinson model that we will show in subsection 4.1.2

According with Zworner *et al.* interpretation there is no change in the frictional force when the velocity goes from $10\,\mathrm{nm/s}$ to $1\,\mu\mathrm{m/s}$. After this, F_{fric} is proportional to γv_c in a viscous damping regime. Our results were done in a wide interval of velocities, covering both previous papers ranges and more, plus a small velocity increment. Displaying the data in a linear scale (Fig. 4.5, left), and with a higher density of points, we can see that the dependence is far from being constant. Moreover, on Fig. 4.5 right, we show how the choice of the scale can influence on the data interpretation, hiding relevant aspects of the behavior of the system.

4.1.1 Small Velocities representation

For small velocities (up to $1\,\mu\mathrm{m/s}$) we also make connections with the results of Fusco and Fasolino [20] by comparing the results of our own simulations with the digitized data from them in Fig. 4.6.

In their article, the authors develop an approximation to the dependence of the frictional force with the velocity, showing that F_{fric} follows a power law of the form:

$$F_{fric} = F_0 + c v_c^{2/3} \tag{4.1}$$

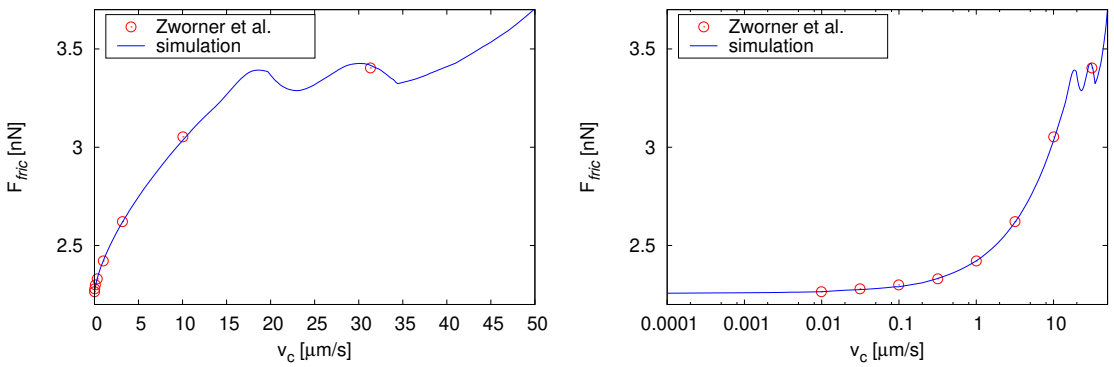

Figure 4.5: Comparison between data from Zworner et al. [64] and from present contribution in linear and semi-log scale.

where c is a constant that depends on the parameter of the model and on the space dimension. This approximation is very accurate for this range of velocities. Highlighting again that the friction is not independent of the velocity. This proves that depending on the scale chosen to represent the data, important information can be overlooked. The same Figure also shows that this power-law dependency continues to be valid for higher velocities of up to $20\,\mu\mathrm{m/s}$.

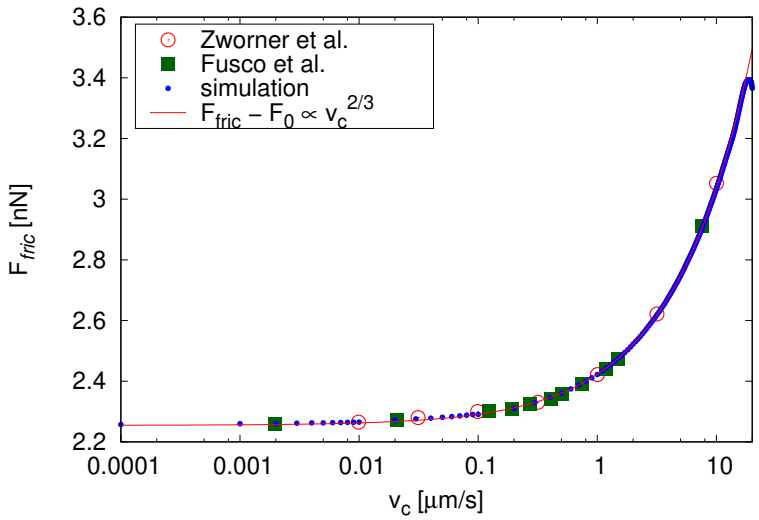

Figure 4.6: Increase of the frictional force with velocity between $10^{-3}\,\mu\mathrm{m/s}$ to $20\,\mu\mathrm{m/s}$. The line is a power-law fit to the data of the form $F_{fric} - F_0 \propto v_c^{2/3}$, from Ref. [20].

4.1.2 Transitional and Large Velocities representation

An important fact that stands out is the distinctive behavior in the region between $10\,\mu\mathrm{m/s}$ and $35\,\mu\mathrm{m/s}$ (Fig. 4.9), where F_{fric} oscillates with v_c around a fixed value of force. Indeed, for the velocities v_c in this region,the tip sees a force from the surface that varies with the a frequency close to its own natural frequency [19, 97], i.e.:

$$v_c^{res} = \frac{a}{2\pi}\sqrt{\frac{k}{m}} \simeq 15\,\mu\mathrm{m/s} \tag{4.2}$$

In order to better understand what could be the origin of the reported behavior we present below the tip position and velocity as a function of the cantilever position (Fig. 4.7 and Fig. 4.8). We present that data for different values of the sliding cantilever velocity. For velocities well below the region where friction oscillates, we have the typical stick-slip behavior where energy dissipates mainly after the slip movement. For large velocities the viscous regime is recovered. However in the region of interest we observe that the tip slips over a distance of two cell parameters, from one potential barrier to the second other one. This happens only for a damping coefficient near critical. Then, instead of being a resonance phenomenon, it is a critical damping effect where the dissipation remains at its minimum compatible with the sliding speed (Fig. 4.8). The presence of double jumps for that range of velocities, makes us to wonder if multiple (more than two) slide jumps would be possible. That can happen, depending on the key parameters of the model, i.e., U_0, k, and a [98], and it deserves a future and thorough analysis.

Such behavior comes to light in reason of the remarkable increase in the density of simulated points and it has not been reported before. In this segment the value of F_{fric} oscillates around an average value of $3.35\,\mathrm{nN}$. This behavior goes totally unnoticed in a logarithmic representation of the data. Some recent experiments [104, 99] have been carried out evaluating the friction dependence on speed near this region, but without covering the entire range and without sufficient detail and precision. In the work of Gangloff [105],the authors also find a similar behavior that they call a friction plateau between between 10^{-3} and $10^{-2}\,\mathrm{m/s}$ and four regimes of friction for an ion-crystal system. The difference with our numerical results is mostly due to the choice of parameters in this contribution.

After the transition region, we observe that friction growths again. We fit the data with

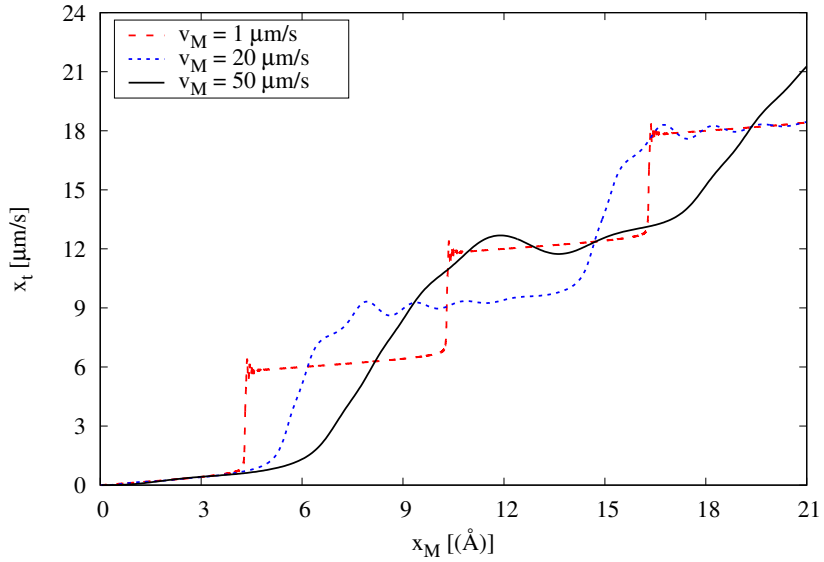

Figure 4.7: Tip position as a function of cantilever position for different sliding velocities, before, at, and after the region where friction oscillates.

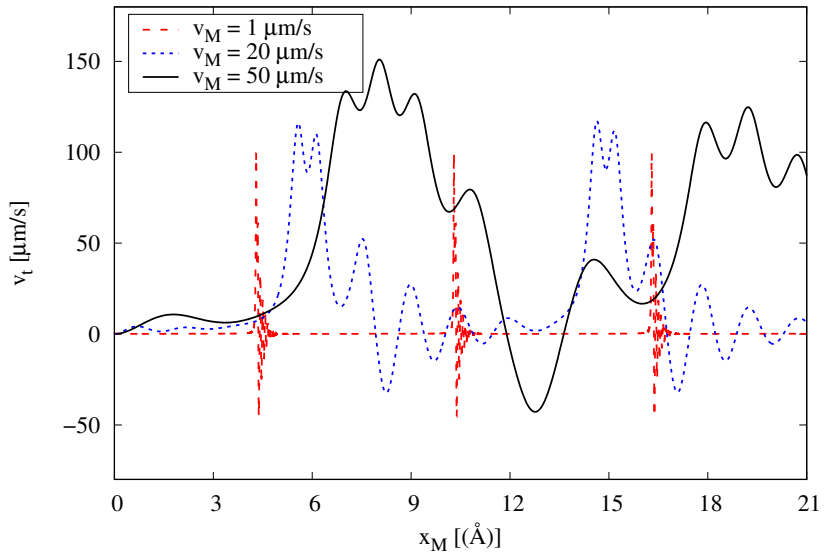

Figure 4.8: Tip velocity as a function of cantilever position for different sliding velocities, before, at, and after the region where friction oscillates.

a quadratic power-law:

$$F_{fric} - F \propto v_c^2 \tag{4.3}$$

where F is the value of the friction at the lower velocity of the adjustment (Fig. 4.10). The quadratic growth fits very well with the simulation data up to $0.1\,\mathrm{mm/s}$ behaving like a drag force until finally, for large sliding velocities, the mechanism of energy dissipation

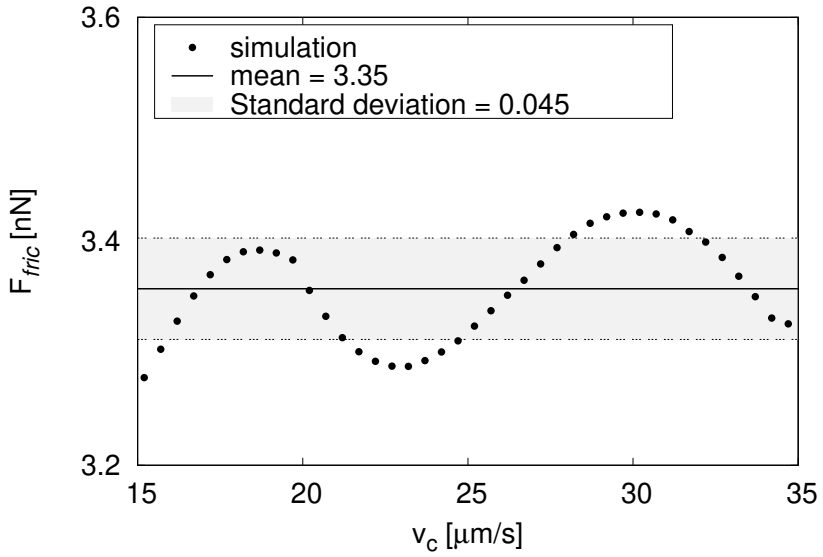

Figure 4.9: Detail of the behavior of the friction force with velocity between 15 to $35\,\mu\mathrm{m/s}$. We can say that friction is stationary in this range of velocities.

through the "stick-slip" effect breaks down, and F_{fric} is proportional to γv_c, where critical damping is assumed, giving $\gamma = 2\sqrt{km}$.

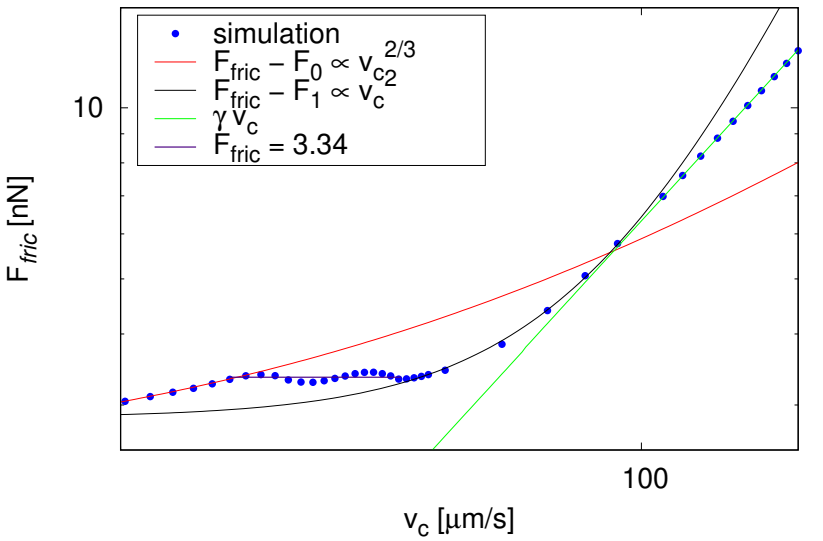

Figure 4.10: The friction force as a function of velocity in the transition region between the low velocities $v_c^{2/3}$ regime to the high velocities, viscous linear regime. For that intermediate regime of velocities the force goes through two other transitional regimes of almost constant force to quadratic velocity regime before entering the linear regime. Increase of the frictional force with velocity between 35 to $100\,\mu\mathrm{m/s}$. The line is a power-law fit to the data of the form $F_{fric} - F \propto v_c^2$. For high velocities the frictional force is proportional to the velocity in the regime of viscous damping

4.2 Two particles interaction

4.2.1 Non Oscillator

First, a non-oscillator or a free particle is consider. By setting $k = 0$ and defining $x = x_f - x_a$ and $X = \frac{m_f x_f + m_a x_a}{m_f + m_a}$ as the internal and center of mass coordinate respectively in Eqs. (3.2) and (3.3), the following equations are obtained:

$$\ddot{x} = \left(\frac{2U_0}{\sigma^2}\right)\left(\frac{1}{m_f} + \frac{1}{m_a}\right) x e^{-x^2/\sigma^2} \tag{4.4}$$

$$\ddot{X} = 0\ . \tag{4.5}$$

Eqs. (4.4) and (4.5) can also be written in terms of conserved quantities as

$$\frac{\dot{x}^2}{2} + U_0\left(\frac{1}{m_f} + \frac{1}{m_a}\right) e^{-x^2/\sigma^2} = \frac{v_0^2}{2} \tag{4.6}$$

$$\dot{X}(t) = \dot{X}(0) = -\frac{v_0 m_f}{m_f + m_a}\ , \tag{4.7}$$

where it is assumed that the two particles are initially well apart from each other, that the free particle starts with velocity $-v_0$ $(v_0 > 0)$ moving to the bound mass, which is initially in equilibrium at rest. With these initial conditions it is straightforward to derive the asymptotic relation between the velocities, when one of the particles has gone far away from the interaction region, i.e., the potential term goes to zero, so from Eq. (4.6-4.7) the next relations are obtained:

$$v_f(\infty) - v_a(\infty) = \pm v_0 \tag{4.8}$$

$$v_f(\infty) + \frac{m_a}{m_f} v_a(\infty) = -v_0\ . \tag{4.9}$$

Combining Eq. (4.8-4.9), the minus sign solution gives $v_a(\infty) = 0$ and $v_f(\infty) = -v_0 = v_f(0)$, so the incoming particle passes through the fixed one, moving away with the same asymptotic velocity it had initially, while the bound one stays at rest after the interaction. Such asymptotic situation, in which the incoming particle does not loose energy after the interaction, happens whenever the initial kinetic energy of the incoming particle is larger

than the maximum of the interaction potential energy, *i.e*:

$$|v_f(0)| > v_{cr} = \sqrt{2U_0 \left(\frac{1}{m_f} + \frac{1}{m_a}\right)} \,. \tag{4.10}$$

The plus sign in Eq. (4.8) gives $v_a(\infty) = \left(\frac{2m_f}{m_f+m_a}\right) v_f(0)$ and $v_f(\infty) = \left(\frac{m_f-m_a}{m_f+m_a}\right) v_f(0)$ as solutions. Therefore, $v_f(\infty)$ can be positive, zero, or negative depending on the relation of the two masses. However, in any case the velocity of m_a is always bigger than the velocity of m_f, meaning that the free particle can not overcome the other when $|v_f(0)| < v_{cr}$. This is the well-known case of elastic collision which, in the center of mass reference system, has a unified description for the three cases, and as such has no relation with the friction related problem we address here. Figure 4.11 shows the final velocity of the free particle as a function of its initial velocity for the case $m_a/m_f = 2$.

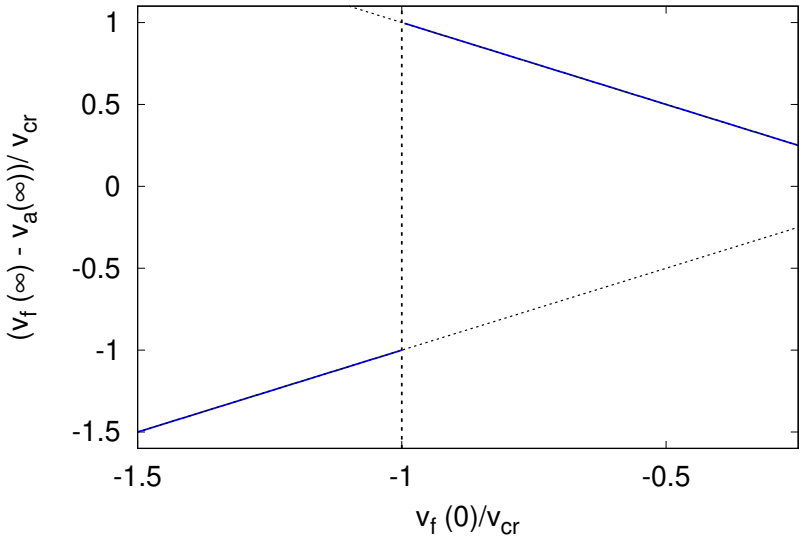

Figure 4.11: Final velocity of the incoming particle, $v_f(\infty)/v_{cr}$, as a function of its initial velocity, $v_f(0)/v_{cr}$ (both in terms of the critical velocity) for the $k = 0$ case. The dashed lines shows the analytic expression and the solid lines are obtained from numerical simulations. The other parameters of the system are $U_0 = 1$ and $\sigma = 1$, m_a is initially at rest ($v_a(0) = 0$) and far from the incoming m_f particle ($v_f(0) = -v_0 < 0$).

4.2.2 Oscillator

The relationship between the initial and final velocities, described before for the case $k = 0$, can become quite complex for $k > 0$, when the second particle is bound to the

equilibrium position of the harmonic potential. In Fig. 4.12 it is shown the dependence of the final velocity of the free particle (m_f) after interacting with the bound particle for three different mass ratios: $\frac{m_a}{m_f} = 2,\ 1$, and 0.5. Different behaviors are observed depending also on the spring constant k being soft, or intermediate.

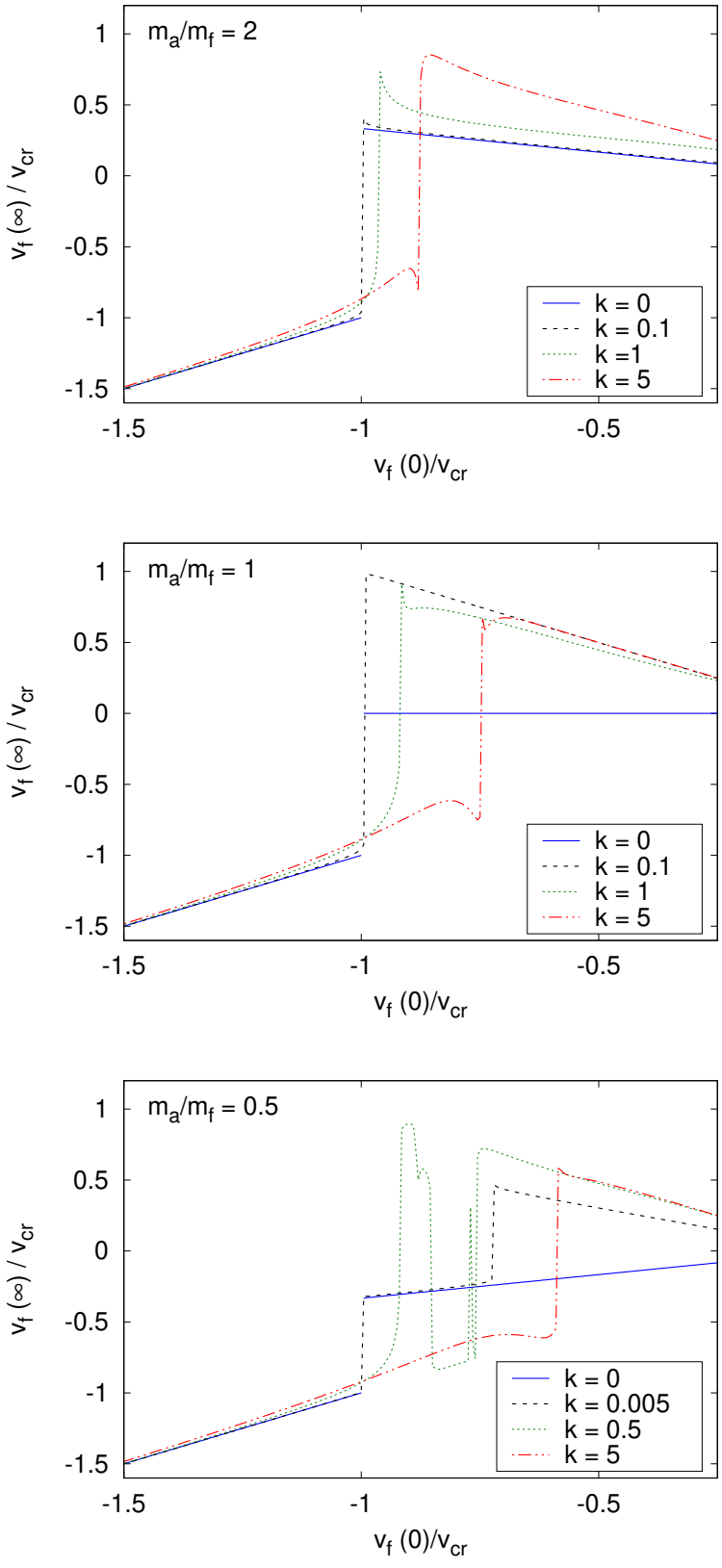

Figure 4.12: Final velocity of the incoming particle, $v_f(\infty)/v_{cr}$, as a function of its initial velocity, $v_f(0)/v_{cr}$ (both in terms of the critical velocity) for the $(k \neq 0)$ case. The other parameters of the system are $U_0 = 1$ and $\sigma = 1$, m_a is initially at rest $(v_a(0) = 0)$ and far from the incoming m_f particle $(v_f(0) = -v_0 < 0)$. Solid (blue) lines show correspond to $(k = 0)$ cases non and have been drawn for reference.

Generally, for large velocities, the free particle overcomes the bound particle with almost no loss of energy, and for low velocities it bounces back, losing some energy which depends on the mass ratio, the value of k, and the initial velocity. Both these situations are not of much interest because they have no implications on the friction problem. Rich and non trivial behavior is observed in the intermediate velocity range, between the $k = 0$ critical velocity and the $k > 0$ critical velocity (which also depends on the mass ratio).

Looking at the upper and central panels of Fig. 4.12, it can be seen that the behavior in the intermediate range of velocities is qualitative similar for different mass ratios, the critical velocity shifts to lower values of $|v|$ as k increases and the energy loss increases with k too. The shift of the critical velocity to lower values when k increases is expected because in the limit of $k \to \infty$ it is recovered the trivial case of fixed potential, with a critical velocity determined by the height of the potential. Let us mention that such extreme case, is of no interest too, because there is no emerging "friction" due to conservation of energy of the m_f particle. Therefore, the exchange of energy between the free and the bound particle is expected to show a maximum at some intermediate k value, as can be seen in Fig. 4.13, which depends on the mass ratio.

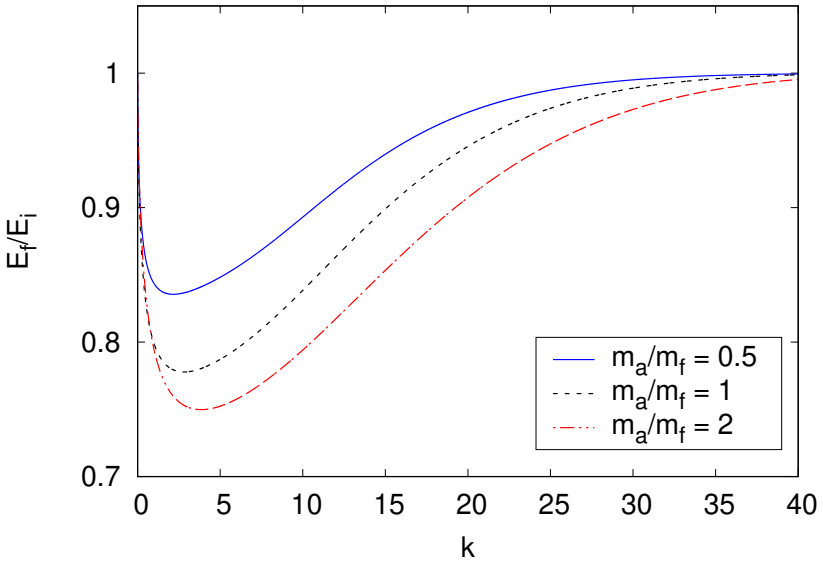

Figure 4.13: Energy ratio vs k for three different mass ratios. The initial velocity of the free particle is $|v_f(0)| = 2$.

Another general behavior observed in Fig. 4.12 is that as the free mass (m_f) increases, relative to the bound mass, the change in the critical velocity becomes more sensitive to the stiffness of the bound particle, k. More precisely, the shift as a function of k is more

dramatic for larger value of the mass m_f. A peculiar situation is observed when the free particle is more massive than the bound one (Fig. 4.12 lower panel), where a complex behavior, with more that one critical velocity, is observed for intermediate values of k. Such a case is discussed in the next section.

4.2.3 Soft k (slow oscillations)

We focus here on the case of soft k which results in slow oscillations of the bound particle. The lower panel of Fig. 4.12 ($m_a/m_f = 0.5$) displays a small window in the initial velocity in which the free particle gets transmitted with a significant loss of energy to the oscillator. Beyond this window the free particle is reflected back. As can be seen in Fig. 4.14 the transition between transmission and reflection exhibits sensitive dependence on the initial conditions. That is, for initial velocities which differ in less than 1 in 10^4, the free particle changes from reflection to transmission. Moreover, the free particle is seen to reflect back with almost the same incoming energy (blue curves in Fig. 4.14). For a slightly larger initial velocity, the free particle is transmitted with less energy than it had initially (red curves in Fig. 4.14). Therefore, in the latter case, much of the energy is transferred into the oscillatory mode of the bound particle. In both situations, however, the two particles interact twice. Such behavior is observed over a range of parameter values.

Since the two collisions are well separated in time, the analysis of the previous section for $k = 0$ can be extended to the two collision observed here for $k \approx 0$. The approximation considers that the two particles move independently (m_f moves at constant velocity and m_a is subject to the harmonic potential) except at the collisions, when the results of the previous section for free particles are applied.

Since the initial velocity of the free particle is less than the critical velocity (v_{cr}) defined in Eq. (4.10), immediately after the first collision $(t > t_1)$ the velocities are:

$$v_f(t_1^+) = \frac{m_f - m_a}{m_f + m_a} v_f(0) \tag{4.11}$$

$$v_a(t_1^+) = \frac{2m_f}{m_f + m_a} v_f(0)\ , \tag{4.12}$$

where, $t_i^{\mp}$ denote the time immediately before and after the collision. Assuming that after

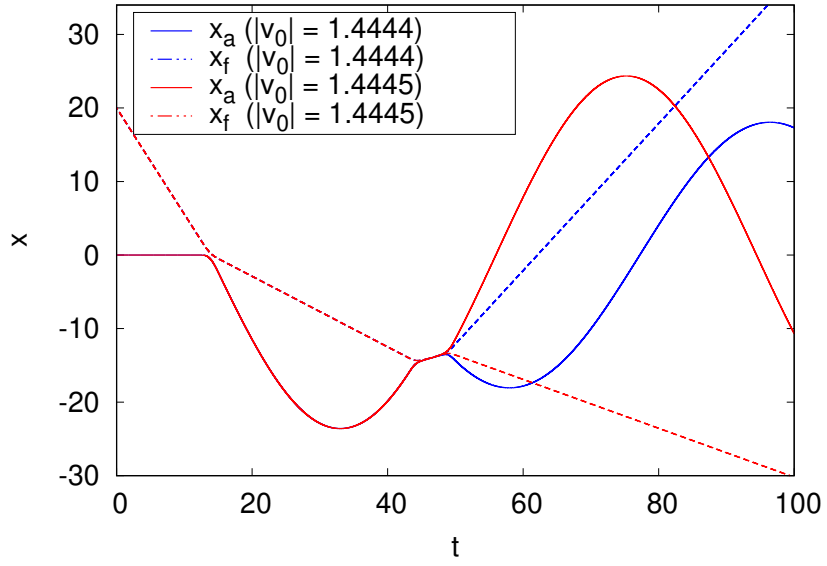

Figure 4.14: Position of the free particle (dashed lines) and the oscillator (solid lines) with reflection (blue lines) or transmission (red lines) of the free particle after interaction with the oscillator. For the reflected case the initial velocity of the free particle is $|v_f(0)| = 1.4444$ and for the transmitted one, it is $|v_f(0)| = 1.4445$. The value of k is taken to be 0.005 and $m_a/m_f = 0.5$. All other parameters are the same as in Fig. 4.12.

this collision, the particles move independently, their position are given by:

$$x_f(t > t_1) = v_f(t_1^+)t \tag{4.13}$$

$$x_a(t > t_1) = sinc(\omega t)v_a(t_1^+)\ . \tag{4.14}$$

So, at the next collision ($t = t_2$), that happens when $x_f(t_2) = x_a(t_2)$, from Eqs. (4.11)-(4.14) the following relation for t_2 holds:

$$sinc(\omega t_2) = \frac{m_f - m_a}{2m_f}\ . \tag{4.15}$$

Transfer of energy between the two is only possible if the velocity of the internal coordinate at this time is less than the critical velocity (v_{cr}). Using Eqs. (4.6), (4.11) and (4.14), the condition on initial velocity for which the behavior of the free particle changes from

transmission to reflection is

$$v_f(0) = \frac{v_{cr}(m_f + m_a)}{m_f(1 - 2\cos(\omega t_2)) - m_a} \ . \tag{4.16}$$

The instantaneous velocity after the second collision can be obtained from conservation of energy and momentum and is given by

$$v_f(t_2^+) = \frac{2m_a}{m_a + m_f} v_a(t_2^-) + \frac{m_f - m_a}{m_a + m_f} v_f(t_2^-) \tag{4.17}$$

$$v_a(t_2^+) = \frac{m_a - m_f}{m_a + m_f} v_a(t_2^-) + \frac{2m_f}{m_a + m_f} v_f(t_2^-) \ . \tag{4.18}$$

Figure 4.15 shows a comparison between the approximate two collision theory and numerical results for $m_a/m_f = 0.5$ and $k = 0.005$. For these parameter values, the different behaviors in the final velocity are distinctly observed and the two collision approximation is able to provide an excellent fit to the numerical results. There is another critical velocity (the intermediate step in Fig. 4.15, or second discontinuity); when the free particle's velocity is larger than this critical velocity, the two particles move with almost the same velocity for a while as if they are stuck together until the elastic force is enough to pull back the bound one and the free particle goes away from it.

Finally, for velocities larger than the critical velocity defined in Eq. 4.10, the free particle goes beyond the oscillator with the same velocity that it came with. In fact, this happens for the three masses relations, showed in Figs. 4.12.

It was shown, in the *Non Oscillator* section, that for equal masses the relation $v_f(t_2^+) = -v_f(0)$ is hold, as it is verified also in the numerical simulations of Fig. 4.12 (middle). Therefore, at the first collision, the free particle transfers its entire energy to the oscillator, which is transferred back to the free particle in the second collision, as showed in Fig. 4.14. Such behavior persist even for relative large values of the oscillator frequency. Even for a heavier free particle, the two collision model shows good qualitative agreement (see Fig. 4.15). The two collision model is not expected to work at higher frequencies since the energy exchange between the two particles cannot be treated as well separated events. However, the approach still provides important insight into the energy exchange between the two particles.

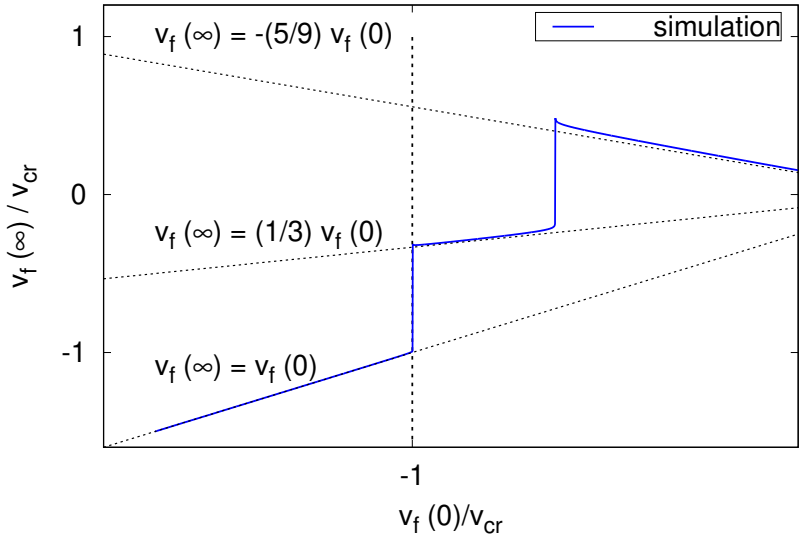

Figure 4.15: Comparison of the results obtained from numerical simulations (solid line) with the approximate two collision analysis (dashed line) for slow oscillations. The value of $k = 0.005$ and $m_a/m_f = 0.5$.

4.2.4 Energy loss calculation

In the previous section, it was shown that the exchange of energy between the two particles depends on the spring constant k and the relative value of their masses. In order to gain some insight into the role of the mass ratio a perturbative approach is presented. Setting the position of the oscillating particle as the perturbation parameter, the Gaussian potential in the equations of motion 3.2 and 3.3 can be expanded up to the first order in x_a. This gives

$$(x_f - x_a)e^{-\frac{(x_f-x_a)^2}{\sigma^2}} = x_f e^{-{x_f}^2/\sigma^2} - x_a(1 - \frac{2x_f^2}{\sigma^2})e^{-x_f^2/\sigma^2} \ . \tag{4.19}$$

Then, the following expressions are obtained

$$\ddot{x}_f = 2c_f x_f e^{-x_f^2/\sigma^2} - 2c_f x_a(1 - 2x_f^2/\sigma^2)e^{-x_f^2/\sigma^2} \tag{4.20}$$

$$\ddot{x}_a = -\frac{k}{m_a}x_a - 2c_a x_f e^{-x_f^2/\sigma^2} \ , \tag{4.21}$$

where $c_f = \frac{U_0}{m_f\sigma^2}$ and $c_a = \frac{U_0}{m_a\sigma^2}$. The free particle moves under the influence of a static potential and the interaction appears as a linear perturbation in the oscillator coordinate

(x_a). Computing the work done by the free particle:

$$\frac{dE}{dt} = F\dot{x}_f = m_f\ddot{x}_f\dot{x}_f \ , \tag{4.22}$$

the following expression is obtained:

$$\frac{dE}{dt} = -2c_f m_f \dot{x}_f x_a (1 - 2x_f^2/\sigma^2) e^{-x_f^2/\sigma^2} + 2c_f m_f x_f \dot{x}_f e^{-x_f^2/\sigma^2} \ . \tag{4.23}$$

The second term in the right hand of Eq. (4.23) changes sign through the collision as x_f goes from $+\infty$ to $-\infty$, so it will be dismissed against the first one. The force due to the static potential is $F(x_f(t)) = c_f m_f x_f e^{-x_f^2/\sigma^2}$ whose derivative with respect to time is $\frac{dF}{dt} = c_f m_f \dot{x}_f (1 - 2x_f^2/\sigma^2) e^{-x_f^2/\sigma^2}$. So the rate of energy loss can be expressed in term of $\frac{dF}{dt}$

$$\frac{dE}{dt} = -2x_a \frac{dF}{dt} \tag{4.24}$$

and the total energy loss, assuming that the free particle is completely transmitted with no rebound, is

$$\Delta E = \int_0^\infty dt \frac{dE}{dt} = -2\int_0^t dt x_a \frac{dF}{dt} = 2\int_0^\infty dt F(x_f(t)) \frac{dx_a}{dt} \ . \tag{4.25}$$

Assuming that $x_a F(t) \to 0$ at infinite, which is true for a pulse. Then, using the formal solution for $x_a(t)$ from Eq. (4.21)

$$\frac{dx_a}{dt} = -\frac{2}{m_a}\int_0^t ds F(x_f(s)) \cos(\omega(t-s)) \tag{4.26}$$

into Eq.4.25, the energy lost by the free particle is

$$\Delta E = -\frac{4}{m_a} \quad \int_0^\infty dt F(x_f(t)) \int_0^t ds F(x_f(s)) cos(\omega(t-s)) \ . \tag{4.27}$$

Fig. 4.16 shows the comparison between the exact solution (continuous line) and the energy ratio obtained by numerically solving Eq. (4.27). $F(x)$ is calculated by taking x solution from Eq. (4.20). The initial velocity of the free particle is kept sufficiently large ($v_f(0) = 4$) to ensure that the free particle is always transmitted. As observed in Fig. 4.16, for small values of σ, the perturbative approach is unable to provide a quantitative estimate

of the velocity and location of the minima, however, for higher σ values the agreement improves and the perturbative approach is able to predict accurately the location of the minima. Independent of the value of σ the approach provides a reaonable qualitative agreement.

As can be seen in Fig. 4.16, the energy ratio has a minimum at a relative low value of the mass ratio ($m_f >> m_a$) meaning the free particle is transmitted losing great part of its energy. It has to be a minimum because in the limit of $m_a \to 0$ there is no particle for the free particle to interact to.

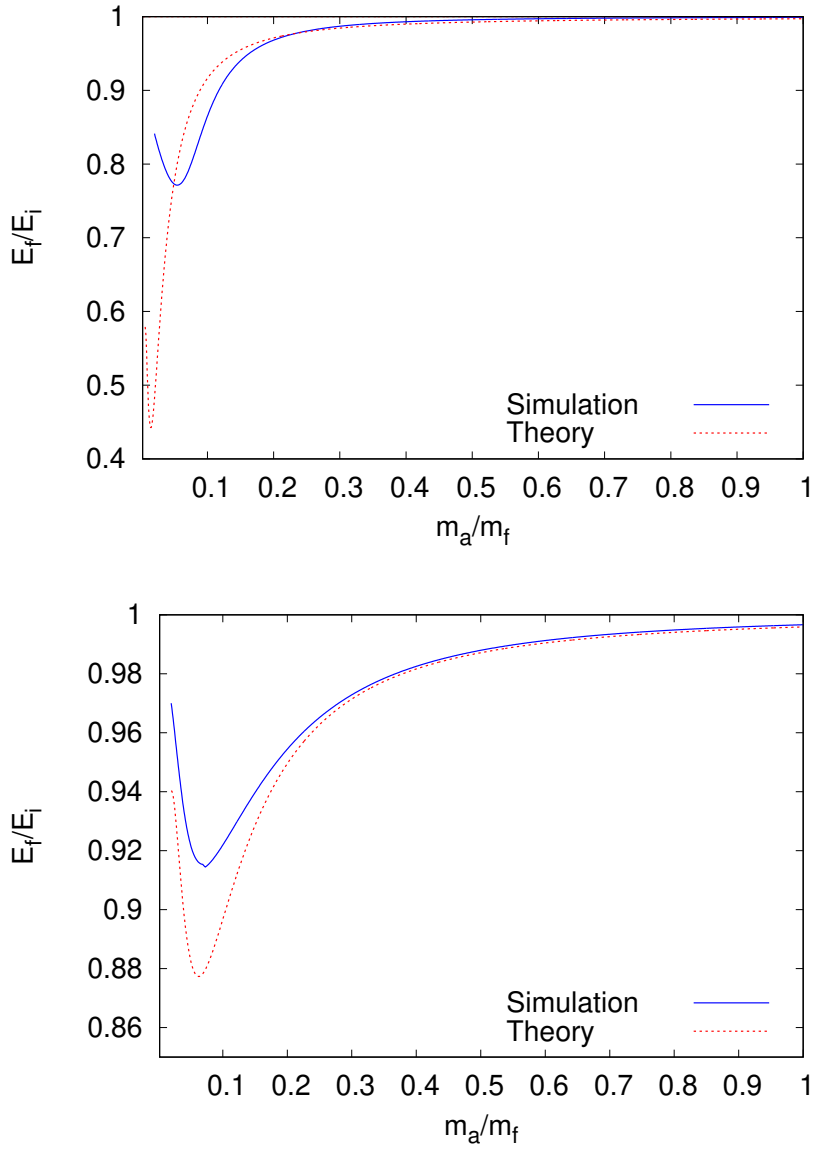

Figure 4.16: Comparison of energy ratio (E_f/E_i) obtained from exact calculation and approximate solution (Eq. 4.27). In both cases the initial velocity of the free particle is $|v_f(0)| = 4$. Top panel if for $\sigma = 1$ and bottom panel for $\sigma = 2$. All other parameters are equal to 1.

4.3 From one to N particles

The problem was solved numerically by using classical molecular-dynamics methods [100, 92] using a set of realistic parameters [64, 20, 39], $m_t = m_s = 10^{-10}\,\mathrm{kg}$, $k_t = k_s = 10\,\mathrm{N/m}$, $a_x = 3$, $U_0 = 0.085\,\mathrm{eV}$, $v_c = 1\,\mu\mathrm{m/s}$ which are typical of an AFM experiments [71, 62]. Te simulations were made for 500 particles and at temperature $T = 0$. The most evident consequence of not having dissipation is that the particles that are perturbed by the tip do not return to their initial state, remaining oscillating infinitely, as it is presented on Fig. 4.17 for the first five particles in dashed lines.

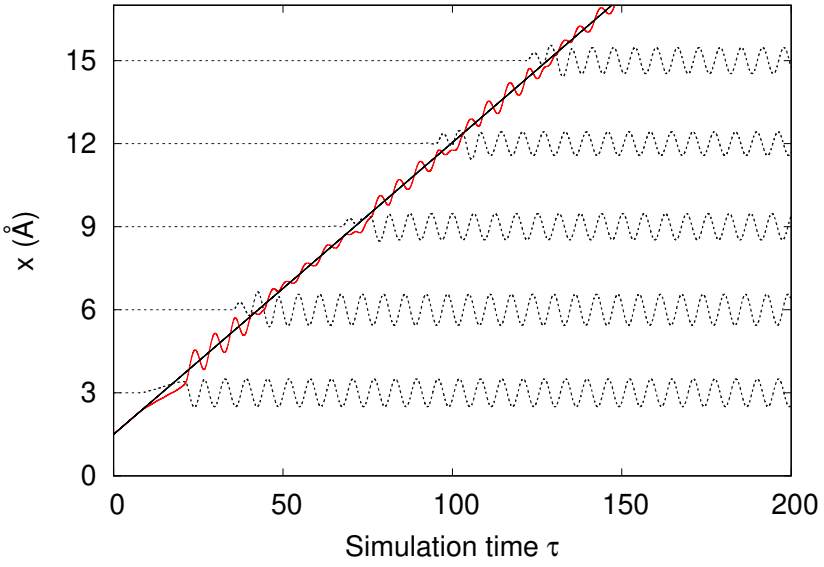

Figure 4.17: Position of the first five particles (dotted lines) after the tip passed through (red line), the black solid line shows the position of the cantilever.

.

For the frictional force calculation we compare three different methods.

It is known that F is defined as the mean value of the lateral force [62, 64, 20, 63]. Since the problem is in one dimension, from here, we will refer to the lateral force as friction force F.

$$F = k_t(X - x) = k_t(X - v_c t) \tag{4.28}$$

The second way to obtain F is through the energy accumulated by the substrate. The power is the instantaneous product of force times velocity and the time derivative of en-

ergy.

$$F\ v_c = \frac{dE}{dt} \tag{4.29}$$

From this relation, it is possible to obtain the frictional force as the slope of the total substrate energy by linear regression. Another method to calculate the friction force in these mechanical problem is calculating the average of the force between the tip and the substrate generated by the Gaussian interaction force. These three methods are compared in Fig. 4.18 with their respective error bars.

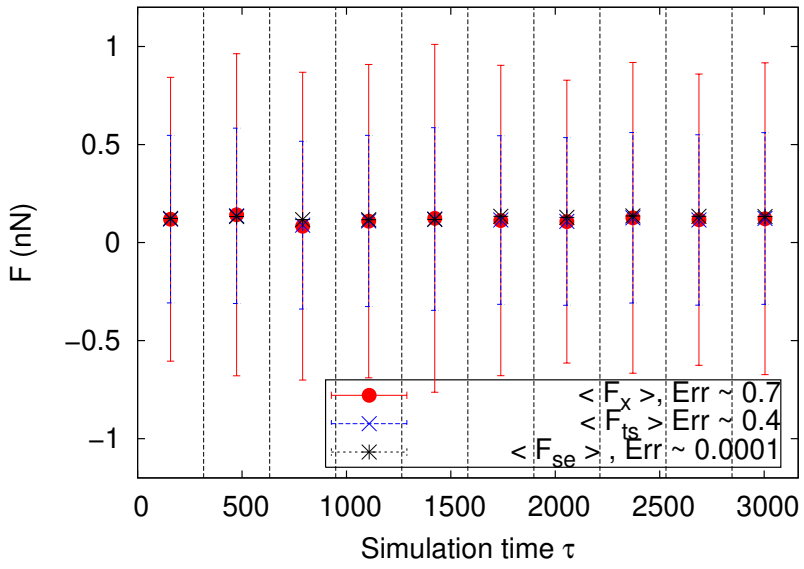

Figure 4.18: Comparison of the friction force values for the three methods of calculation, and their respective error bars.

.

The total simulation time τ was divided into ten equal regions. For each of these intervals, the mean of the force was calculated in order to compare their values. $\langle F_x \rangle$ represents the value obtained from Eq. 3.8, $\langle F_{ts} \rangle$ from the Gaussian potential between the tip and the substrate; and $\langle F_{se} \rangle$ is the slope of the accumulated energy of the substrate.

In Fig. 4.19 it is shown the accumulation of energy by the substrate and the values of the frictional force obtained by the three methods. In this case, τ was divided into three regions.

The comparison of the three methods shows that the smallest error in the measurements corresponds to the force obtained through the energy accumulated by the substrate.

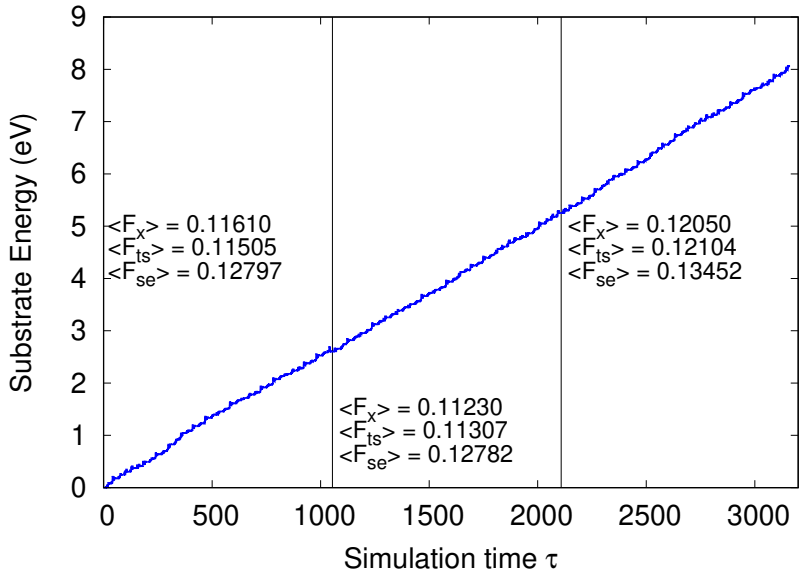

Figure 4.19: Comparison of the lateral force values for the three methods in different times

.

For this reason, we have chosen it to perform the rest of the simulations where all the parameters of the model will be analyzed.

4.3.1 Time step comparison

Molecular dynamics simulation is a technique by which, step by step, the equations of motion that describe the Newton's classical mechanics are solved [100, 101, 92]. In the process of integrating the equations, the common important parameter is the time step Δt. If a big time step is chosen, the MD simulation becomes unstable due to the very big error in the integration process, not showing behaviors existing in the mechanical problem. If the time step is very small, the simulation will not be efficient due to a very long calculation time.

Earlier works [103, 102] have been demonstrated that stable dynamics will be executed only with the use of the smaller time step compared to the period of the highest vibrational frequency. Determining the biggest time step for a stable dynamics, will maximize the efficiency of the molecular dynamics simulation.

For these reason and since every mechanical problem is different from each other we decide to solve the equations for several time steps in order to choose the indicated such that not take long simulation time but at the same time we can extract reliable results referring to the lateral force.

Fig. 4.20 shows the energy of the substrate (kinetic energy plus elastic potential energy) for different Δt :from 0.001 to 10 [ns]. As we are interested in getting the value of F_x from the slope of the curve, it can be observed that the choose of higher or lower time steps doesn't affect significantly the final result. The difference can be visualized in graphs such as position,velocity or F_x itself, where for small values of Δt, oscillations of the tip are missing. In conclusion, for the numerical simulations we choose $\Delta t = 0.1ns$,since the computational time required is not very high and this value does not allow any behavior of the tip to go unnoticed.

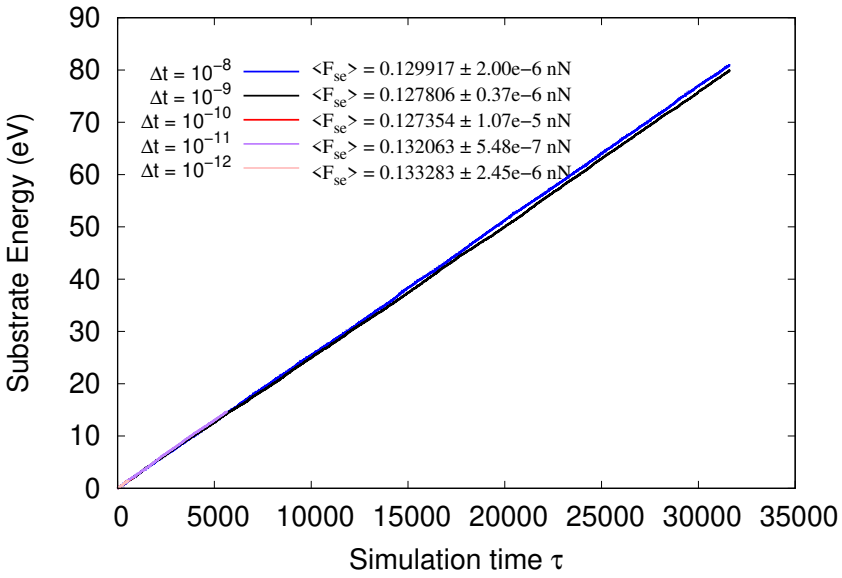

Figure 4.20: Substrate energy for different different time-steps.

.

Once the method and the time step have been chosen, we calculate F varying each of the parameters of the model. The variation of F with the velocity of the driven support it is shown in Fig. 4.21. For small velocities $v_c < 1\,\mu\mathrm{m}$, F remains constant and for higher values, it drops to zero. This is expected since the model does not have a velocity-dependent damping term. The total energy of the substrate decreases as the support velocity increases because the tip does not interact enough time with the substrate particles. As a consequence, the amplitude of oscillation around the equilibrium position is not significant.

When the variable parameter is the elasticity k_s of the substrate particles (Fig. 4.22), we can identify a behavior of the shape $F = 1/k_s^n$ in three different regions. For the first interval, k_s <1 $\mathrm{N/m}$, the adjustment parameter is $n = 1$. This means that as k_s increases,

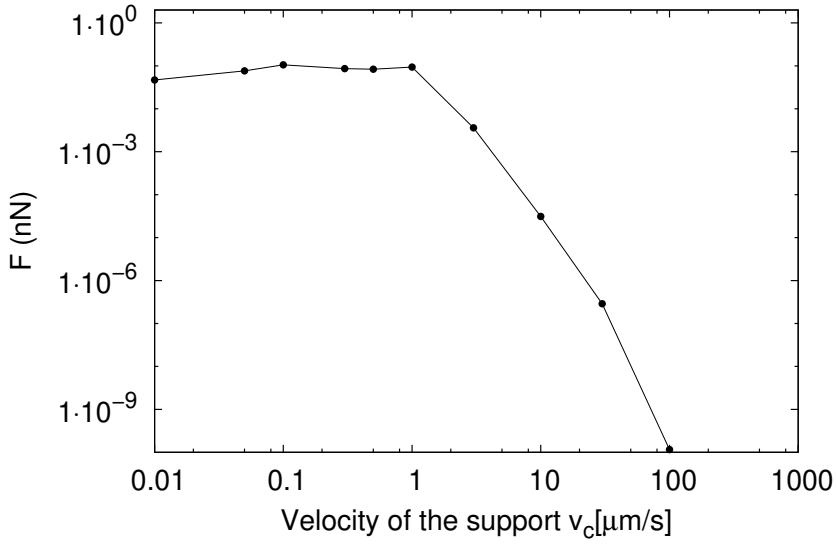

Figure 4.21: Lateral Friction Force in function of the velocity of the cantilever. The other parameters were $m_t = m_s = 10^{-10}\,\mathrm{kg}$, $k_t = k_s = 10\,\mathrm{N/m}$, $a_x = 3$, $U_0 = 0.085\,\mathrm{eV}$

.

F decreases. The softer the material, the higher the energy lost. When $1\,\mathrm{N/m} < k_s < 130\,\mathrm{N/m}$ there is an unpredictable region with maximums and minimums. Although there is an oscillation in the values of the friction, we assume that the average value remains constant. For that reason, the parameter $n \approx 0.26$. The third region, shows a more expected result. Due to the hardness of the substrate, the particles do not deviate from their equilibrium position, so the elastic potential is almost null as well as the kinetic energy. In these region, the parameter $n = 4$.

The variation of the friction with corrugation U_0, reproduced in Fig. 4.23, follows the shape $F = mU_0$, where again m varies for three different regions. Performing linear regression we could find the values of m for each of these. In this case, since the data is better visualized and interpreted in linear scale, we did not see the need to represent the results in logarithmic scale. It can be observed that F increase with the high of potential energy following the shape when U_0 is up to $0.5\,\mathrm{eV}$, $m \approx 1.81$. The friction almost doubles its value for each increment in U_0. For the second region, the growth rate decreases to a quarter of the presented in the first interval, here $m \approx 0.46$. And for the third range, the growth is already very small, taking into account that it represents the eighth part of the first region growth. This is because the tip remains in between two particles for more time (while the support advances), as the amplitude increases.

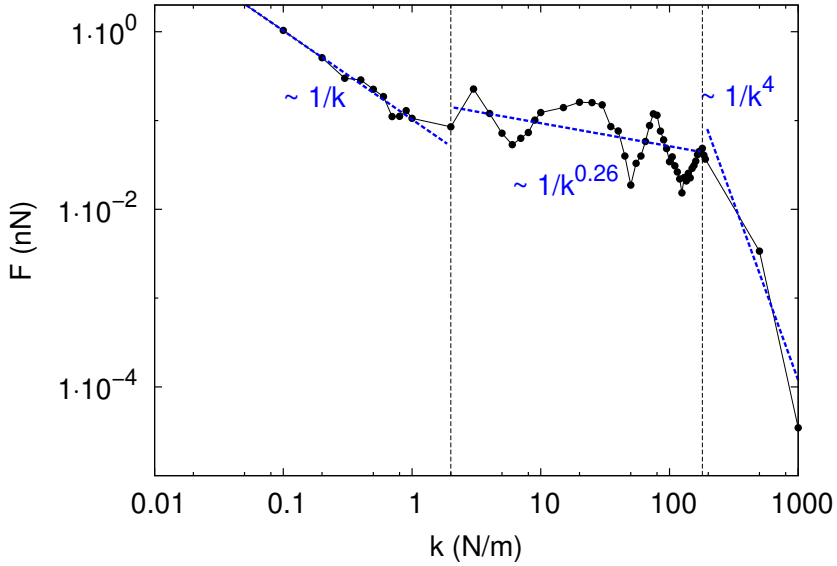

Figure 4.22: Lateral Friction Force with substrate spring stiffness. The rest of the parameters were $m_t = m_s = 10^{-10}\,\mathrm{kg}$, $k_t = 10\,\mathrm{N/m}$, $a_x = 3$, $U_0 = 0.085\,\mathrm{eV}$, $v_c = 1\,\mu\mathrm{m/s}$, the dotted vertical lines indicate the three behavior regimes.

.

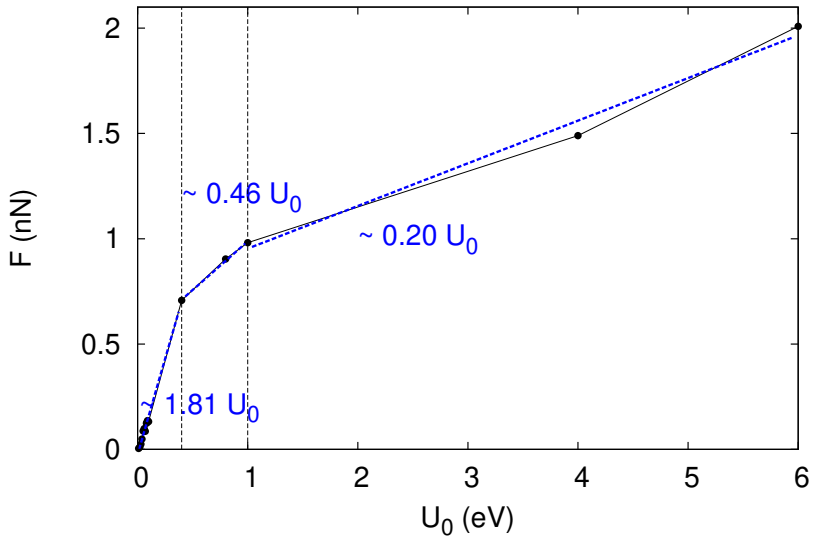

Figure 4.23: Lateral Friction Force in function of the potential high. The other parameters were: $m_t = m_s = 10^{-10}\,\mathrm{kg}$, $k_t = k_s = 10\,\mathrm{N/m}$, $a_x = 3$, $v_c = 1\,\mu\mathrm{m/s}$,the dotted vertical lines indicate the three behavior regimes.

.

The last Figure correspond to the friction force behavior with the mass ratio between the particles of the substrate and the tip m_s/m_t (Fig. 4.24). We can see that when $m_s < m_t$ the frictional force maintains its constant value, then begins to decrease until reaching a

minimum, corresponding to $m_s = 2m_t$. After this point increases again and for a small gap of values between $m_s = 5m_t$ and $m_s = 10m_t$ again F shows independent on the masses ratio. Finally, fall to zero for very large substrate masses. When the masses are too big, the potential energy of the substrate is very small since the mass of the tip does not manage to move them.

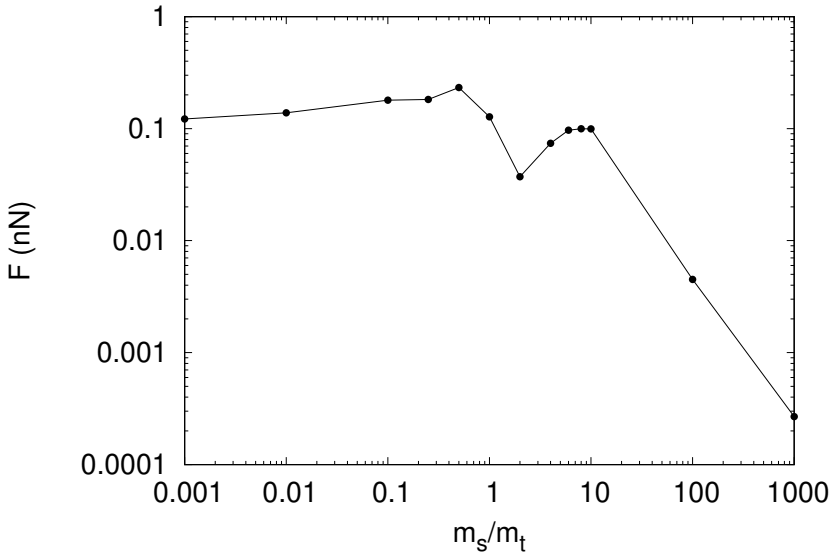

Figure 4.24: Lateral Friction Force in function of the masses ratio. The other parameters were: k_t = k_s = 10 N/m, a_x = 3 , U_0 = 0.085 eV, v_c = 1 μm/s.

.

4.4 Single interaction and periodic lattice equivalence

The remarkable thing of the results presented in section 4.2, for the first simple model of Fig. 3.1 is that an effective dissipation emerges from the point of view of the incoming particle which we postulate as a possible mechanism involved in the macroscopic friction.

In order to link such interpretation with the second model proposed in Fig. 3.2 we calculate the friction using the same parameters of the two particle system.

The friction force F_x was obtained through the Eq. (the energy accumulated by the substrate)

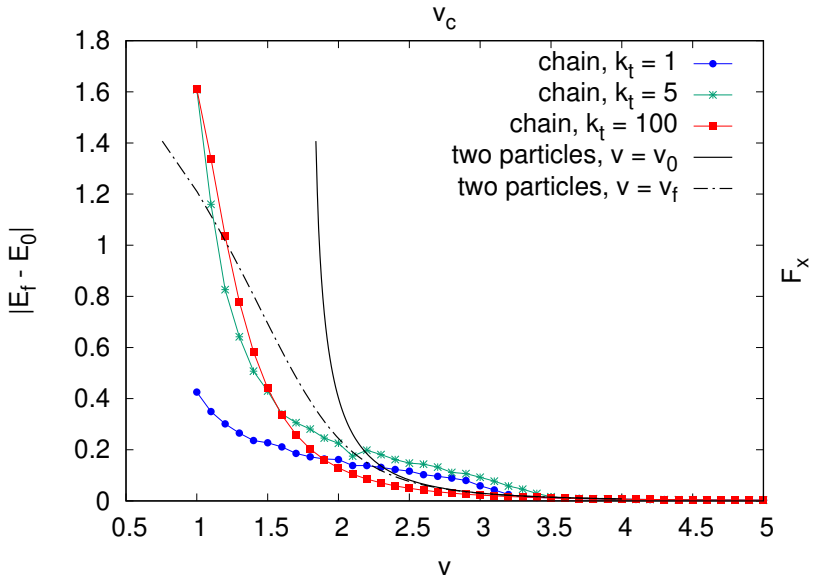

Figure 4.25: Absolute energy loss $|E_f - E_0|$ as function of initial and final velocity for the two particles interaction (dashed and solid line) and friction force F_x as function of the cantilever velocity v_c for the tip-substrate interaction. The effect of three well different stiffness k_t is evaluated, while the rest of the parameters are equal to 1.

Fig. 4.25 show the results of the numerical simulations for the tip-substrate interaction (dotted lines) and for two particles interaction (dashed and solid line). The results show that the stiffer the k_t, the particle behaves as a free particle sliding over the substrate without any constraint. F_x in the limit case (when $k_t = 100$), presents the same behavior as the energy loss by the free particle in the case of the simplified system. It can be noticed that the curve is dislocated to the left, that is, the force is much greater in the chain for lower tip velocities. This is due to two reasons, the first is that the tip particle always moves at the same constant speed (unlike the first model, where it was thrown with an initial velocity) and the second is that throughout its course interacts with all the particles

of the substrate. With these final results we can consolidate the main idea of this work and demonstrate that the transfer of energy from the incoming particle to the confined one can be regarded as the emerging dissipation force of the system.

Chapter 5

Conclusions

This doctoral thesis aimed to study several aspects in regards to the frictional force. The first part was dedicated to revisit the Prandtl-Tomlinson model and thus compare the results obtained with those of previous works, especially with respect to the behavior of friction with velocity.

We have presented a thorough numerical study. Despite the fact that similar works have already been carried out, our contribution was made for a higher velocity range and for a bigger density of points, bringing to light behaviors not previously reported for this model. By comparing our results with previous ones with the same model we were able to conciliate apparent conflicting results while providing new insight and interpretation of them. Besides, we present results in regions not previously explored. We confirm Fusco and Fasolino results for small velocities but extended up to $15\,\mu\mathrm{m/s}$, where friction force has a dependency of $v_c^{2/3}$. A transition region located between 15-35 $\mu\mathrm{m/s}$ where assume a constant average frictional force and then an increase proportional to v_c^2 up to about $100\,\mu\mathrm{m/s}$. After this, the force is proportional to γv_c in a viscous damping regime. Our numerical study shows that depending on how the results are presented, mainly when changing from linear scale to logarithmic, part of this rich an interesting behavior can go unnoticed.

However, what we consider to be the main contribution is the fact that we have studied a system where we do not put the *ad-hoc* dissipation from the beginning, and work the model with conservation of energy. We made a simpler first version with only two particles –one with initial velocity thrown against other confined in a harmonic potential– and studied the regime in which the collision between these particles, because of the Gaussian

potential, can give in transmission or reflection, and in some cases an intercalation of both situations.

Despite its simplicity, the model shows effective dissipation on the free particle movement as a result of the interaction with the bound one. The free particle, that can be regarded as a model simplification of an adsorbate, asperity, or a tip, moves past the bound particle (a simplification of a substrate) with less energy than it has before the interaction. the energy goes to the bound particles which remain oscillating after the interaction, representative of the heating of the substrate. The non-linearity of the potential plus the constraint in the bound particle are the key elements for this emerging behavior to appear.

Finally we studied the model with a periodic network and we were able to find a equivalence between the energy transmitted to the network (i.e. a transmitted energy in the form of phonons) and the friction force and we found that the behavior as a function of the velocity of the incident particle is similar .

Bibliography

[1] B. N. J. Persson. *Sliding Friction*. Springer Berlin Heidelberg, 2000. doi: 10.1007/978-3-662-04283-0. URL http://dx.doi.org/10.1007/978-3-662-04283-0.

[2] J. Krim. Surface science and the atomic-scale origins of friction: what once was old is new again. *Surface Science*, 500(1–3):741 – 758, 2002. ISSN 0039-6028. doi: https://doi.org/10.1016/S0039-6028(01)01529-1. URL http://www.sciencedirect.com/science/article/pii/S0039602801015291.

[3] L. Makkonen. A thermodynamic model of sliding friction. *AIP Advances*, 2(1): 012179, 2012. doi: 10.1063/1.3699027. URL http://dx.doi.org/10.1063/1.3699027.

[4] Great Britain Department of Education, Science. Lubrication Engineering (Education, and Research) Working Group. *Lubrication (tribology) : education and research; a report on the present position and industry's needs.* London : H.M.S.O., 1966. URL http://copac.jisc.ac.uk/id/1171591?style=html&title=Lubrication%20(tribology)education%20and%20research%3B%20a%20report.

[5] H. P. Jost. Tribology — origin and future. *Wear*, 136(1):1 – 17, 1990. ISSN 0043-1648. doi: http://dx.doi.org/10.1016/0043-1648(90)90068-L. URL http://www.sciencedirect.com/science/article/pii/004316489090068L.

[6] I. L. Singer and H. M. Pollock. Epilogue to The NATO ASI on Fundamentals of Friction. In *Fundamentals of Friction: Macroscopic and Micro-*

scopic Processes, pages 569–588. Springer Science Business Media, 1992. doi: 10.1007/978-94-011-2811-7_29. URL http://dx.doi.org/10.1007/978-94-011-2811-7_29.

[7] G. Heinrich and M. Klüppel. Rubber friction, tread deformation and tire traction. *Wear*, 265(7):1052 – 1060, 2008. ISSN 0043-1648. doi: http://dx.doi.org/10.1016/j.wear.2008.02.016. URL http://www.sciencedirect.com/science/article/pii/S0043164808000847.

[8] R. J. Pinnington. Rubber friction on rough and smooth surfaces. *Wear*, 267(9): 1653 – 1664, 2009. ISSN 0043-1648. doi: http://dx.doi.org/10.1016/j.wear.2009.06.011. URL http://www.sciencedirect.com/science/article/pii/S0043164809004220.

[9] A. L. Gal, L. Guy, G. Orange, Y. Bomal, and M. Klüppel. Modelling of sliding friction for carbon black and silica filled elastomers on road tracks. *Wear*, 264(7): 606 – 615, 2008. ISSN 0043-1648. doi: http://dx.doi.org/10.1016/j.wear.2007.05.002. URL http://www.sciencedirect.com/science/article/pii/S0043164807005340.

[10] J. Krim. Friction at the atomic scale. *Scientific American*, 275(4):74–80, 1996.

[11] R. Bennewitz. Friction force microscopy. *Materials Today*, 8(5): 42 – 48, 2005. ISSN 1369-7021. doi: http://dx.doi.org/10.1016/S1369-7021(05)00845-X. URL http://www.sciencedirect.com/science/article/pii/S136970210500845X.

[12] A. Buldum and S. Ciraci. Atomic-scale study of dry sliding friction. *Phys. Rev. B*, 55:2606–2611, Jan 1997. doi: 10.1103/PhysRevB.55.2606. URL http://link.aps.org/doi/10.1103/PhysRevB.55.2606.

[13] L. Prandtl. Ein Gedankenmodell zur kinetischen Theorie der festen Körper. *ZAMM - Zeitschrift für Angewandte Mathematik und Mechanik*, 8(2):85–106, 1928. doi: 10.1002/zamm.19280080202. URL http://dx.doi.org/10.1002/zamm.19280080202.

[14] G. A. Tomlinson. CVI. A molecular theory of friction. *The London Edinburgh, and Dublin Philosophical Magazine and Journal of Science*, 7(46):905–939, jun 1929. doi: 10.1080/14786440608564819. URL http://dx.doi.org/10.1080/14786440608564819.

[15] T. Kontorova and J. Frenkel. On the theory of plastic deformation and twinning. II. *Zh. Eksp. Teor. Fiz.*, 8:1340–1348, 1938. URL http://cds.cern.ch/record/431596.

[16] J. Frenkel and T. Kontorova. On the theory of plastic deformation and twinning. *Izv. Akad. Nauk, Ser. Fiz.*, 1:137–149, 1939. URL http://cds.cern.ch/record/431595.

[17] O. M. Braun and Y. S. Kivshar. *The Frenkel-Kontorova Model: Concepts, Methods, and Applications*. Physics and Astronomy Online Library. Springer, 2004. ISBN 9783540407713. URL https://books.google.com.br/books?id=zyoT068mu0YC.

[18] S. Gonçalves, V. M. Kenkre, and A. R. Bishop. Nonlinear friction of a damped dimer sliding on a periodic substrate. *Phys. Rev. B*, 70(19), nov 2004. doi: 10.1103/physrevb.70.195415. URL http://dx.doi.org/10.1103/physrevb.70.195415.

[19] S. Gonçalves, C. Fusco, A. R. Bishop, and V. M. Kenkre. Bistability and hysteresis in the sliding friction of a dimer. *Phys. Rev. B*, 72:195418, Nov 2005. doi: 10.1103/PhysRevB.72.195418. URL https://link.aps.org/doi/10.1103/PhysRevB.72.195418.

[20] C. Fusco and A. Fasolino. Velocity dependence of atomic-scale friction: A comparative study of the one- and two-dimensional Tomlinson model. *Phys. Rev. B*, 71 (4), jan 2005. doi: 10.1103/physrevb.71.045413. URL http://dx.doi.org/10.1103/physrevb.71.045413.

[21] M. Tiwari, S. Gonçalves, and V. M. Kenkre. Generalization of a nonlinear friction relation for a dimer sliding on a periodic substrate. *The European Physical Journal B*, 62(4):459–464, apr 2008. doi: 10.1140/epjb/e2008-00194-9. URL http://dx.doi.org/10.1140/epjb/e2008-00194-9.

[22] E. A. Salcedo Torres Tese de Doutorado: Modelo unidimensional do atrito em escala atômica : um estudo por dinâmica molecular ,2006. Instituto de Física - Universidade Federal do Rio Grande do Sul-RS-Brasil

[23] I. G. Neide Tese de Doutorado: Efeitos rotacionais no atrito não linear de um dímero deslizando sobre um substrato periódico unidimensional ,2011. Instituto de Física - Universidade Federal do Rio Grande do Sul-RS-Brasil

[24] I. G. Neide, V. M. Kenkre, and S. Gonçalves. Effects of rotation on the nonlinear friction of a damped dimer sliding on a periodic substrate. *Physical Review E*, 82 (4), oct 2010. doi: 10.1103/physreve.82.046601. URL http://dx.doi.org/10.1103/physreve.82.046601.

[25] E. S. Torres, S. Gonçalves, C.Scherer and M. Kiwi. Nanoscale sliding friction versus commensuration ratio: Molecular dynamics simulations. *Physical Review B*, 73(3), Jan 2006. doi: 10.1103/PhysRevB.73.035434. URL https://link.aps.org/doi/10.1103/PhysRevB.73.035434.

[26] B. N. J. Persson. *Sliding Friction: Physical Principles and Applications*. NanoScience and Technology. Springer Berlin Heidelberg, 2013. ISBN 9783662042830. URL https://books.google.com.br/books?id=KFb-CAAAQBAJ.

[27] A. Fall, B. Weber, M. Pakpour, N. Lenoir, N. Shahidzadeh, J. Fiscina, C. Wagner, and D. Bonn. Sliding Friction on Wet and Dry Sand. *Phys. Rev. Lett.*, 112(17), apr 2014. doi: 10.1103/physrevlett.112.175502. URL http://dx.doi.org/10.1103/physrevlett.112.175502.

[28] J. E. Fiscina, M. Pakpour, A. Fall, N. Vandewalle, C. Wagner, and D. Bonn. Dissipation in quasistatically sheared wet and dry sand under confinement. *Physical Review E*, 86(2), aug 2012. doi: 10.1103/physreve.86.020103. URL http://dx.doi.org/10.1103/physreve.86.020103.

[29] J. Duran, A. Reisinger and P. G. de Gennes. Sands, Powders, and Grains: An Introduction to the Physics of Granular Materials. Partially Ordered Systems, Springer New York. 2012 ISBN 9781461204992

[30] D. Dowson. *History of Tribology*. Longman, 1979. ISBN 9780582447660. URL https://books.google.com.br/books?id=t-sNAQAAIAAJ.

[31] F. P. Bowden. The Friction and Lubrication of Solids. *Am. J. Phys.*, 19(7):428, 1951. doi: 10.1119/1.1933017. URL http://dx.doi.org/10.1119/1.1933017.

[32] V. Popov. *Contact Mechanics and Friction: Physical Principles and Applications*. Springer Berlin Heidelberg, 2010. ISBN 9783642108037. URL https://books.google.com.br/books?id=-I8qtcJN1VIC.

[33] T. Baumberger Dry Friction Dynamics at Low Velocities. *Persson B.N.J., Tosatti E. (eds) Physics of Sliding Friction. NATO ASI Series (Series E: Applied Sciences)*, vol 311. Springer, Dordrecht

[34] J. F. Archard. Elastic deformation and the laws of friction. *Proceedings of the Royal Society of London. Series A, Mathematical and Physical Sciences*, 243(1233): 190–205, 1957. ISSN 00804630. URL http://www.jstor.org/stable/100445.

[35] J. A. Greenwood and J. B. P. Williamson. Contact of Nominally Flat Surfaces. *Proceedings of the Royal Society A: Mathematical Physical and Engineering Sciences*, 295(1442):300–319, dec 1966. doi: 10.1098/rspa.1966.0242. URL http://dx.doi.org/10.1098/rspa.1966.0242.

[36] B. N. J. Persson. Adhesion between an elastic body and a randomly rough hard surface. *The European Physical Journal E*, 8(4):385–401, Jul 2002. doi: 10.1140/epje/i2002-10025-1. URL https://doi.org/10.1140/epje/i2002-10025-1.

[37] E. Gnecco, R. Bennewitz, T. Gyalog, Ch. Loppacher, M. Bammerlin, E. Meyer, and H.-J. Güntherodt. Velocity Dependence of Atomic Friction. *Phys. Rev. Lett.*, 84(6):1172–1175, feb 2000. doi: 10.1103/physrevlett.84.1172. URL http://dx.doi.org/10.1103/physrevlett.84.1172.

[38] Y.Hu, T. Ma, and H. Wang. Energy dissipation in atomic-scale friction. *Friction*,

1(1):24–40, 2013. ISSN 2223-7704. doi: 10.1007/s40544-013-0002-6. URL http://dx.doi.org/10.1007/s40544-013-0002-6.

[39] Z. Wang, T. Ma, Y. Hu, L. Xu, and H. Wang. Energy dissipation of atomic-scale friction based on one-dimensional prandtl-tomlinson model. *Friction*, 3(2):170–182, 2015. ISSN 2223-7704. doi: 10.1007/s40544-015-0086-2. URL http://dx.doi.org/10.1007/s40544-015-0086-2.

[40] B. Bhushan. Nanotribology Nanomechanics and Materials Characterization. In *Nanotribology and Nanomechanics*, pages 311–416. Springer Science Business Media, 2008. doi: 10.1007/978-3-540-77608-6_8. URL http://dx.doi.org/10.1007/978-3-540-77608-6_8.

[41] H. Holscher, A. Schirmeisen, and U. D Schwarz. Principles of atomic friction: from sticking atoms to superlubric sliding. *Philosophical Transactions of the Royal Society A: Mathematical Physical and Engineering Sciences*, 366(1869): 1383–1404, apr 2008. doi: 10.1098/rsta.2007.2164. URL http://dx.doi.org/10.1098/rsta.2007.2164.

[42] J. Filla, C. Aguzzoli, V. Sonda, M.C.M. Farias, G.V. Soares, I.J.R. Baumvol and C.A. Figueroa Nanoscale friction of partially oxidized silicon nitride thin films. *Surface and Coatings Technology*, 205(19):4528 - 4531, 2011. doi: https://doi.org/10.1016/j.surfcoat.2011.03.111. URL http://www.sciencedirect.com/science/article/pii/S0257897211003008.

[43] A.L. Bandeira, R. Trentin, C. Aguzzoli, M.E.H. Maia da Costa, A.F. Michels, I.J.R. Baumvol, M.C.M. Farias and C.A. Figueroa Sliding wear and friction behavior of CrN-coating in ethanol and oil–ethanol mixture. *Wear*, 301(1):786 - 794, 2013. doi: https://doi.org/10.1016/j.wear.2013.01.111. URL http://www.sciencedirect.com/science/article/pii/S0043164813001336.

[44] B. Bhushan, J. N. Israelachvili, and U. Landman. Nanotribology: friction wear and lubrication at the atomic scale. *Nature*, 374(6523):607–616, apr 1995. doi: 10.1038/374607a0. URL http://dx.doi.org/10.1038/374607a0.

[45] B. Bhushan. Nanotribology and nanomechanics. *Wear*, 259(7-12):1507–1531, jul 2005. doi: 10.1016/j.wear.2005.01.010. URL http://dx.doi.org/10.1016/j.wear.2005.01.010.

[46] G. Binnig and H. Rohrer. Scanning tunneling microscopy-from birth to adolescence. *Reviews of Modern Physics*, 59(3):615–625, jul 1987. doi: 10.1103/revmodphys.59.615. URL http://dx.doi.org/10.1103/revmodphys.59.615.

[47] G. Binnig, C. F. Quate, and Ch. Gerber. Atomic Force Microscope. *Phys. Rev. Lett.*, 56(9):930–933, mar 1986. doi: 10.1103/physrevlett.56.930. URL http://dx.doi.org/10.1103/physrevlett.56.930.

[48] T. Gyalog and H. Thomas. Atomic friction. *Zeitschrift für Physik B Condensed Matter*, 104(4):669–674, dec 1997. doi: 10.1007/s002570050506. URL http://dx.doi.org/10.1007/s002570050506.

[49] T. Gyalog, E. Gnecco, and E. Meyer. Stick-Slip Motion on the Atomic Scale. In *Fundamentals of Friction and Wear*, pages 101–115. Springer Science Business Media, 2007. doi: 10.1007/978-3-540-36807-6_6. URL http://dx.doi.org/10.1007/978-3-540-36807-6_6.

[50] A. Volmer and T. Nattermann. Towards a statistical theory of solid dry friction. *Zeitschrift für Physik B Condensed Matter*, 104(2):363–371, jun 1997. doi: 10.1007/s002570050462. URL http://dx.doi.org/10.1007/s002570050462.

[51] J. Krim and A. Widom. Damping of a crystal oscillator by an adsorbed monolayer and its relation to interfacial viscosity. *Phys. Rev. B*, 38:12184–12189, Dec 1988. doi: 10.1103/PhysRevB.38.12184. URL https://link.aps.org/doi/10.1103/PhysRevB.38.12184.

[52] H.S. Nalwa. *Handbook of Nanostructured Materials and Nanotechnology, Five-Volume Set*. Elsevier Science, 1999. ISBN 9780080533643. URL https://books.google.com.br/books?id=dzl6xahWI7EC.

[53] C. M. Mate, G. M. McClelland, R. Erlandsson, and S. Chiang. Atomic-scale friction of a tungsten tip on a graphite surface. *Phys. Rev. Lett.*, 59:1942–1945, Oct 1987. doi: 10.1103/PhysRevLett.59.1942. URL http://link.aps.org/doi/10.1103/PhysRevLett.59.1942.

[54] S. Fujisawa, E. Kishi, Y. Sugawara, and S. Morita. Atomic-scale friction observed with a two-dimensional frictional-force microscope. *Phys. Rev. B*, 51:7849–7857, Mar 1995. doi: 10.1103/PhysRevB.51.7849. URL https://link.aps.org/doi/10.1103/PhysRevB.51.7849.

[55] L. Prandtl. Über flüssigkeitsbewegung bei sehr kleiner reibung,verhandlungen iii. *Intern. Math. Kongress, Heidelberg*, page 484, 1904.

[56] L. Prandtl. Über die härte plastischer körper. *Nachrichten Göttinger Akad. Wiss,*, 1920.

[57] M. H. Müser,M. Urbakh,M. O. Robbins Statistical mechanics of static and low-velocity kinetic friction. In: Prigogine, I., Rice, S.A. (eds.) Advances in Chemical Physics, vol. 126, pp. 187–272,2003.

[58] V. Popov, and J. A. T. Gray Prandtl-Tomlinson Model: A Simple Model Which Made History, ISBN 978-3-642-39904-6 153–168, jan 2014

[59] J. J. Mazo, D. Dietzel, A. Schirmeisen, J. G. Vilhena, and E. Gnecco. Time strengthening of crystal nanocontacts. *Phys. Rev. Lett.*, 118:246101, Jun 2017. doi: 10.1103/PhysRevLett.118.246101. URL https://link.aps.org/doi/10.1103/PhysRevLett.118.246101.

[60] D. Tománek, W. Zhong, and H. Thomas. Calculation of an Atomically Modulated Friction Force in Atomic-Force Microscopy. *Europhysics Letters (EPL)*, 15(8): 887–892, aug 1991. doi: 10.1209/0295-5075/15/8/014. URL http://dx.doi.org/10.1209/0295-5075/15/8/014.

[61] T. Gyalog and H. Thomas. Mechanism of Atomic Friction. In *Physics of Sliding Friction*, pages 403–413. Springer Science Business Media, 1996. doi: 10.1007/978-94-015-8705-1_24. URL http://dx.doi.org/10.1007/978-94-015-8705-1_24.

[62] H. Hölscher, U.D. Schwarz, and R. Wiesendanger. Modelling of the scan process in lateral force microscopy. *Surface Science*, 375(2-3):395–402, apr 1997. doi: 10.1016/s0039-6028(96)01285-x. URL http://dx.doi.org/10.1016/s0039-6028(96)01285-x.

[63] J. S. Helman, W. Baltensperger, and J. A. Hol/yst. Simple model for dry friction. *Phys. Rev. B*, 49(6):3831–3838, feb 1994. doi: 10.1103/physrevb.49.3831. URL http://dx.doi.org/10.1103/physrevb.49.3831.

[64] O. Zworner, H. Holscher, U.D. Schwarz, and R. Wiesendanger. The velocity dependence of frictional forces in point-contact friction. *Applied Physics A: Materials Science & Processing*, 66(7):S263–S267, mar 1998. doi: 10.1007/s003390051142. URL http://dx.doi.org/10.1007/s003390051142.

[65] B. Lorenz, Y. R. Oh, S. K. Nam, S. H. Jeon, and B. N. J. Persson. Rubber friction on road surfaces: Experiment and theory for low sliding speeds. *The Journal of Chemical Physics*, 142(19):194701, 2015. doi: 10.1063/1.4919221. URL http://dx.doi.org/10.1063/1.4919221.

[66] A. Socoliuc, R. Bennewitz, E. Gnecco, and E. Meyer. Transition from Stick-Slip to Continuous Sliding in Atomic Friction: Entering a New Regime of Ultralow Friction. *Phys. Rev. Lett.*, 92(13), apr 2004. doi: 10.1103/physrevlett.92.134301. URL http://dx.doi.org/10.1103/physrevlett.92.134301.

[67] T. Bouhacina, J. P. Aimé, S. Gauthier, D. Michel, and V. Heroguez. Tribological behavior of a polymer grafted on silanized silica probed with a nanotip. *Phys. Rev. B*, 56:7694–7703, Sep 1997. doi: 10.1103/PhysRevB.56.7694. URL https://link.aps.org/doi/10.1103/PhysRevB.56.7694.

[68] M. L. Iglesias and S. Gonçalves Sliding and Dry Friction: Prandtl-Tomlinson Athermal Model Revisited *Brazilian Journal of Physics*,2018 doi: 10.1007/s13538-018-0610-8to be publish

[69] Maria Lujan Iglesias, Sebastian Goncalves, V.M. Kenkre, Mukesh Tiwari Energy exchange in a two particles system,2018 arXiv:1707.05910

[70] M. L. Iglesias and S. Gonçalves. Tomlinson model improved with no ad-hoc dissipation,2018 arXiv:1708.03415 work in progress

[71] R. Bennewitz, T. Gyalog, M. Guggisberg, M. Bammerlin, E. Meyer, and H.-J. Güntherodt. Atomic-scale stick-slip processes on cu(111). *Phys. Rev. B*, 60: R11301–R11304, Oct 1999. doi: 10.1103/PhysRevB.60.R11301. URL http://link.aps.org/doi/10.1103/PhysRevB.60.R11301.

[72] E. Riedo, E. Gnecco, R. Bennewitz, E. Meyer, and H. Brune. Interaction potential and hopping dynamics governing sliding friction. *Phys. Rev. Lett.*, 91:084502, Aug 2003. doi: 10.1103/PhysRevLett.91.084502. URL http://link.aps.org/doi/10.1103/PhysRevLett.91.084502.

[73] Q. Li, Y. Dong, D. Perez, A. Martini, and R. W. Carpick. Speed dependence of atomic stick-slip friction in optimally matched experiments and molecular dynamics simulations. *Phys. Rev. Lett.*, 106:126101, Mar 2011. doi: 10.1103/PhysRevLett.106.126101. URL http://link.aps.org/doi/10.1103/PhysRevLett.106.126101.

[74] K. B. Jinesh, S. Yu. Krylov, H. Valk, M. Dienwiebel, and J. W. M. Frenken. Thermolubricity in atomic-scale friction. *Phys. Rev. B*, 78:155440, Oct 2008. doi: 10.1103/PhysRevB.78.155440. URL http://link.aps.org/doi/10.1103/PhysRevB.78.155440.

[75] Y. Sang, M. Dubé, and M. Grant. Thermal effects on atomic friction. *Phys. Rev. Lett.*, 87:174301, Oct 2001. doi: 10.1103/PhysRevLett.87.174301. URL http://link.aps.org/doi/10.1103/PhysRevLett.87.174301.

[76] K. Y. S. Braun O. M. Nonlinear dynamics of the frenkel–kontorova model. *Physics Reports*, 306(1-2):1–108, 1998. doi: 10.1016/s0370-1573(98)00029-5.

[77] L. M. Floría and J. J. Mazo. Dissipative dynamics of the frenkel-kontorova model. *Advances in Physics*, 45(6):505–598, 1996. doi: 10.1080/00018739600101557. URL https://doi.org/10.1080/00018739600101557.

[78] S. Watanabe, H. S.J. van der Zant, S. H. Strogatz, and T. P. Orlando. Dynamics of circular arrays of josephson junctions and the discrete sine-gordon equa-

tion. *Physica D: Nonlinear Phenomena*, 97(4):429 – 470, 1996. ISSN 0167-2789. doi: https://doi.org/10.1016/0167-2789(96)00083-8. URL http://www.sciencedirect.com/science/article/pii/0167278996000838.

[79] S. N. Coppersmith and D. S. Fisher. Threshold behavior of a driven incommensurate harmonic chain. *Phys. Rev. A*, 38:6338–6350, Dec 1988. doi: 10.1103/PhysRevA.38.6338. URL https://link.aps.org/doi/10.1103/PhysRevA.38.6338.

[80] M. Peyrard and M. D. Kruskal. Kink dynamics in the highly discrete sine-gordon system. *Physica D: Nonlinear Phenomena*, 14(1):88 – 102, 1984. ISSN 0167-2789. doi: https://doi.org/10.1016/0167-2789(84)90006-X. URL http://www.sciencedirect.com/science/article/pii/016727898490006X.

[81] K. Shinjo and M. Hirano. Dynamics of friction: superlubric state. *Surface Science*, 283(1):473 – 478, 1993. ISSN 0039-6028. doi: https://doi.org/10.1016/0039-6028(93)91022-H. URL http://www.sciencedirect.com/science/article/pii/003960289391022H.

[82] A. V. Ustinov, M. Cirillo, and B. A. Malomed. Fluxon dynamics in one-dimensional josephson-junction arrays. *Phys. Rev. B*, 47:8357–8360, Apr 1993. doi: 10.1103/PhysRevB.47.8357. URL https://link.aps.org/doi/10.1103/PhysRevB.47.8357.

[83] O.M. Braun and Y.S. Kivshar. *The Frenkel-Kontorova Model: Concepts, Methods, and Applications*. Theoretical and Mathematical Physics. Springer Berlin Heidelberg, 2013. ISBN 9783662103319. URL https://books.google.com.br/books?id=fWvrCAAAQBAJ.

[84] T. Strunz and F.-J. Elmer. Driven frenkel-kontorova model. i. uniform sliding states and dynamical domains of different particle densities. *Phys. Rev. E*, 58:1601–1611, Aug 1998. doi: 10.1103/PhysRevE.58.1601. URL https://link.aps.org/doi/10.1103/PhysRevE.58.1601.

[85] E. D. Smith, M. O. Robbins, and M. Cieplak Friction on adsorbed monolayers. *Phys. Rev. B*, 54:(11)8252–8260, Sep. 1996. doi: 10.1103/PhysRevB.54.8252. URL https://link.aps.org/doi/10.1103/PhysRevB.54.8252.

[86] M. S. Tomassone, J. B. Sokoloff, A. Widom, and J. Krim Dominance of Phonon Friction for a Xenon Film on a Silver (111) Surface. *Phys. Rev. Lett.*, 79:(24)4798–4801, Dec. 1997. doi: 10.1103/PhysRevLett.79.4798. URL https://link.aps.org/doi/10.1103/PhysRevLett.79.4798.

[87] A. Liebsch, S. Gonçalves, and M. Kiwi Electronic versus phononic friction of xenon on silver. *Phys. Rev. B*, 60:(7)5034–5043, Aug. 1999. doi: 10.1103/PhysRevB.60.5034. URL https://link.aps.org/doi/10.1103/PhysRevB.60.5034.

[88] S. R. Sales de Mello, M. E. H. Maia da Costa, C. M. Menezes, C. D. Boeira, F. L. Freire Jr, F. Alvarez and C. A. Figueroa On the phonon dissipation contribution to nanoscale friction by direct contact. *Scientific Reports*, 3242:(7)2045-2322, 2017. doi: 10.1038/s41598-017-03046-8. URL https://doi.org/10.1038/s41598-017-03046-8.

[89] R. Scott, M. P. Allen, and D. J. Tildesley. Computer Simulation of Liquids. *Mathematics of Computation*, 57(195):442, jul 1991. doi: 10.2307/2938686. URL http://dx.doi.org/10.2307/2938686.

[90] M. O. Robbins and M. H. Müser. Computer Simulations of Friction, Lubrication and Wear. *eprint arXiv:cond-mat/0001056*, January 2000.

[91] M. P. Allen, D. J. Tildesley, and Jayanth R. Banavar. Computer Simulation of Liquids. *Phys. Today*, 42(3):105, 1989. doi: 10.1063/1.2810937. URL http://dx.doi.org/10.1063/1.2810937.

[92] D. Frenkel and B. Smit. *Molecular Dynamics Simulations*. Elsevier BV, 2002. doi: 10.1016/b978-012267351-1/50006-7. URL http://dx.doi.org/10.1016/b978-012267351-1/50006-7.

[93] L. VERLET. Computer Experiments on Classical Fluids. II. Equilibrium Correlation Functions. *Phys. Rev.*, 165(1):201–214, jan 1968. doi: 10.1103/physrev.165.201. URL http://dx.doi.org/10.1103/physrev.165.201.

[94] H. C. J. Berendsen and W. F. van Gunsteren. *Dynamics Simulation of*

Statistical-Mechanical Systems. G. P. F. Ciccotti and W. G. Hoover (North Holland,Amsterdam, 1986.

[95] P. Procacci and M. Marchi. *Advances in the Computer Simulations of Liquid Crystals*. Kluwer Academic Publishers.

[96] Engauge Digitizer, https://markummitchell.github.io/engauge-digitizer/, note = Accessed: 2018-09-24

[97] J. Ciccoianni, G. Riva, R. Capozza, R. L. Woulaché, N. Manini C. Apostoli and G. Giusti Velocity dependence of sliding friction on a crystalline surface. *Beilstein J.Nanotechnol.*, 8:2186–2199, 2017. doi: 10.3762/bjnano.8.218.

[98] E. Gnecco, R. Roth, and A. Baratoff, Analytical expressions for the kinetic friction in the Prandtl-Tomlinson model Phys. Rev. B 86, 035443, 2012.

[99] Y. Diao and R. Espinosa-Marzal. The role of water in fault lubrication. 9, 12 2018.

[100] D. J. Allen, M. P.; Tildesley. *Computer Simulation of Liquids*. Oxford, 1987.

[101] D. C. Rapaport. *The Art of Molecular Dynamics Simulation*. Cambridge Univ. Press, 1995.

[102] J.-I. Choe and B. Kim. Determination of proper time step for molecular dynamics simulation. 21, 04 2000.

[103] H. Grubmüller and P. Tavan. Multiple time step algorithms for molecular dynamics simulations of proteins: How good are they? *J. Comput. Chem.*, 19(13):1534–1552, 1998.

[104] J. Chen, I. Ratera, J. Y. Park, and M. Salmeron. Velocity dependence of friction and hydrogen bonding effects. *Phys. Rev. Lett.*, 96:236102, Jun 2006. doi: 10.1103/PhysRevLett.96.236102. URL https://link.aps.org/doi/10.1103/PhysRevLett.96.236102.

[105] D. Gangloff, A. Bylinskii, I. Counts, W. Jhe, V. Vuletić. Velocity tuning of friction with two trapped atoms. *Nature Physics*, 11:915, Sep 2015. doi: 10.1038/nphys3459. URL https://doi.org/10.1038/nphys3459.